

An exact theory of three-dimensional fixed separation in unsteady flows

Amit Surana,¹ Gustaaf B. Jacobs,² Oliver Grunberg,¹ and George Haller^{1,a)}

¹*Department of Mechanical Engineering, Massachusetts Institute of Technology, Cambridge, Massachusetts 02139, USA*

²*Department of Aerospace Engineering and Engineering Mechanics, San Diego State University, San Diego, California 92182, USA*

(Received 24 July 2007; accepted 25 July 2008; published online 8 October 2008)

We develop a nonlinear theory for separation and attachment on no-slip boundaries of three-dimensional unsteady flows that have a steady mean component. In such flows, separation and attachment surfaces turn out to originate from fixed lines on the boundary, even though the surfaces themselves deform in time. The exact separation geometry is not captured by instantaneous Eulerian fields associated with the velocity field, but can be determined from a weighted average of the wall-shear and wall-density fields. To illustrate our results, we locate separation surfaces and attachment surfaces in an unsteady model flow and in direct numerical simulations of a time-periodic lid-driven cavity. © 2008 American Institute of Physics. [DOI: 10.1063/1.2988321]

I. INTRODUCTION

In this paper, we derive criteria for flow separation on no-slip boundaries in unsteady velocity fields with a steady mean. By unsteady flow with a steady mean, we mean a fluid velocity field that is the sum of a steady component and zero-mean oscillations. The time dependence of these oscillations is arbitrary, as long as their asymptotic average is zero.

Separation in unsteady flows can be defined in different ways; here we adopt the view of Prandtl, who states that at the separation location “a fluid-sheet projects itself into the free flow.” In other words, we seek to identify the location of material spikes that transport particles from the vicinity of the boundary to other flow regions.

Material spike formation and associated particle ejection may take place within a boundary layer (local separation or separation bubble formation), out of a boundary layer (boundary-layer separation), or even in the absence of a boundary layer (separation in Stokes flows). Our objective is to develop wall-based criteria that predict spike formation in all these cases regardless of the magnitude of the Reynolds number. This approach continues the rigorous study of three-dimensional flow separation initiated by Surana *et al.*¹ for steady flows.

A. Prior work on three-dimensional unsteady separation

As opposed to two-dimensional flows that separate at isolated boundary points, three-dimensional (3D) flows tend to separate from the boundary along lines, not isolated wall-shear zeros. This increased complexity makes the detection of 3D separation a challenging task (see Refs. 2–5, for reviews).

In Surana *et al.*,¹ we developed a mathematically exact theory of 3D separation for steady flows. We identified separation

lines and angles in terms of the wall-shear and wall-pressure fields. We also gave a full classification of all observable separation geometries. Since we assumed steadiness for the flow, our Lagrangian-based proofs rendered separation and attachment surfaces that coincided with distinguished stream surfaces emanating from the wall.

For unsteady velocity fields, the Lagrangian and Eulerian descriptions of separation differ. The wall-shear distribution, a prominent on-wall signature of separation, becomes time dependent. As a result, classical techniques, such as critical point theory for autonomous vector fields, become inapplicable to the analysis of near-wall behavior. In fact, applying such techniques to instantaneous wall-shear fields leads to incorrect results, as two-dimensional examples show.^{6–8} In general, instantaneous Eulerian descriptions fail to yield a self-consistent and rigorous approach to unsteady flow separation.

On the other hand, the Lagrangian approach has been notably successful in describing 3D unsteady separation in the boundary-layer equations. Continuing the two-dimensional work of Shen⁹ and Van Dommelen and Shen,¹⁰ Van Dommelen and Cowley¹¹ derived Lagrangian criteria for the formation of material spikes, which they attribute to a finite-time blow-up in Prandtl’s boundary-layer equation.

Even though the above approach has been highly influential in the boundary-layer literature, linking separation to singularities in the boundary-layer equations raises as many questions as it answers. First, rigorous mathematical examples show that even the steady boundary-layer equations can display fluid breakaway without any singularity formation at the breakaway point.¹² Second, unsteady boundary-layer equations can develop singularities without any obvious connection with separation.¹³ Third, while material spikes do form in physical Navier–Stokes flows, singularities are generally agreed to be absent. Fourth, computing Lagrangian conditions at off-wall locations, as required by Lagrangian boundary-layer-separation theory, appears unrealistic in an experimental implementation.

^{a)}Author to whom correspondence should be addressed. Electronic mail: ghaller@mit.edu.

An alternative Lagrangian approach to unsteady separation in Navier–Stokes flows was proposed by Wu *et al.*,^{14,15} who viewed separation as a distinguished 3D motion of particles near the boundary. Working with instantaneous particle motion, they derived conditions for the simultaneous convergence and upwelling of fluid near general boundaries. These conditions are physically appealing and give reasonable results for the prolate spheroid example considered in Ref. 15. Still, they lack a rigorous mathematical foundation and, in general, give inaccurate separation locations away from zero-wall-shear points even for steady flows.¹

B. Main results

Here we develop an extension of the results of Surana *et al.*¹ on steady separation to *fixed unsteady separation* in 3D flows. By fixed unsteady separation, we mean fluid departure from the boundary near time-independent lines on the boundary. Such fixed separation lines might seem counterintuitive for an unsteady flow, but turn out to be ubiquitous in flows with a temporal mean component. In such flows, oscillations of the velocity field around its mean give rise to well-defined averaged locations where particles break away from the boundary. The surfaces that these particles follow, however, have general time dependence.

In nonlinear dynamical system terms, fixed unsteady flow separation takes place along a *nonhyperbolic unstable manifold* emanating from the no-slip boundary.^{8,16} In 3D, such an unstable manifold is either a one-dimensional time-dependent material curve (*separation curve*) or a two-dimensional time-dependent material surface (*separation surface*). Both of these material structures collect and eject particles from the vicinity of the boundary; in backward time, they both shrink to the boundary. They deform in time, but their base on the boundary cannot move along the boundary because of the no-slip boundary conditions.

To locate separation curves and surfaces in unsteady flow with a steady mean, we apply the mathematical theory of averaging.¹⁷ Averaging is applicable here because in appropriate local coordinates, the differential equation for Lagrangian particle motion becomes slowly varying near the boundary. In these coordinates, averaging theory allows us to derive mathematically exact criteria for wall-based unstable manifolds. Despite their unsteadiness, separation curves and surfaces have a steady base that remains fixed on the no-slip boundary. We predict these fixed locations by applying the steady 3D separation criteria of Surana *et al.*¹ to a weighted average of the wall-shear field. We also obtain leading-order approximations for the time-varying separation curves and surfaces near the wall.

The separation theory we derive in this paper is exact in the following sense:

- (1) We specify the class of flows we consider (Sec. II): flows with a well-defined steady mean component.
- (2) We summarize commonly observed physical properties of the separation surface that we explicitly use in our analysis (Sec. III): local uniqueness, nonzero angle enclosed with the wall, smoothness, and robustness under small perturbation (i.e., observability in experiments).

- (3) We derive exact analytical expressions (theorems) for the location and shape of separation and attachment surfaces with the above properties. We give detailed proofs in Appendices A and D.

We illustrate our analytic predictions on a randomly oscillating separation bubble model and on a direct numerical simulation of a time-periodic lid-driven cavity flow.

II. SETUP AND ASSUMPTIONS

Consider a 3D unsteady velocity field,

$$\mathbf{v}(x, y, z, t) = [u(x, y, z, t), v(x, y, z, t), w(x, y, z, t)], \quad (1)$$

with a flat stationary boundary at $z=0$; a treatment of general curved boundaries is similar.¹⁸ Throughout this paper, we shall assume that \mathbf{v} is continuously differentiable.

On the $z=0$ boundary, the velocity field satisfies the no-slip boundary condition

$$u(x, y, 0, t) = v(x, y, 0, t) = w(x, y, 0, t) = 0. \quad (2)$$

To distinguish the velocity components parallel to the boundary, we let $\mathbf{x}=(x, y)$, so that

$$\mathbf{u}(\mathbf{x}, z, t) = [u(x, y, z, t), v(x, y, z, t)],$$

$$w(\mathbf{x}, z, t) = w(x, y, z, t).$$

We shall denote the wall-tangential spatial gradient by $\nabla_{\mathbf{x}} = \mathbf{e}_x \partial_x + \mathbf{e}_y \partial_y$, where \mathbf{e}_x and \mathbf{e}_y are unit vectors along the x and y axes.

If the velocity field is mass conserving and admits no sinks or sources on the boundary, then the fluid density ρ satisfies the continuity equation

$$\partial_t \rho + \nabla \cdot (\rho \mathbf{v}) = 0. \quad (3)$$

On the $z=0$ boundary, the no-slip boundary conditions simplify Eq. (3) to the linear differential equation,

$$\partial_t \rho(\mathbf{x}, 0, t) + \rho(\mathbf{x}, 0, t) \partial_z w(\mathbf{x}, 0, t) = 0$$

for $\rho(\mathbf{x}, 0, t)$; the solution to this equation is

$$\rho(\mathbf{x}, 0, t) = \rho(\mathbf{x}, 0, t_0) e^{-\int_{t_0}^t \partial_z w(\mathbf{x}, 0, s) ds}. \quad (4)$$

Taking the gradient of Eq. (4) gives the wall-tangential density-gradient evolution,

$$\begin{aligned} \nabla_{\mathbf{x}} \rho(\mathbf{x}, 0, t) &= \nabla_{\mathbf{x}} \rho(\mathbf{x}, 0, t_0) e^{-\int_{t_0}^t \partial_z w(\mathbf{x}, 0, s) ds} \\ &\quad - \rho(\mathbf{x}, 0, t_0) e^{-\int_{t_0}^t \partial_z w(\mathbf{x}, 0, s) ds} \int_{t_0}^t \nabla_{\mathbf{x}} \partial_z w(\mathbf{x}, 0, s) ds. \end{aligned} \quad (5)$$

Assuming that the density and density gradient of the fluid remain bounded from below and from above for all times, we obtain from Eqs. (4) and (5) the estimates

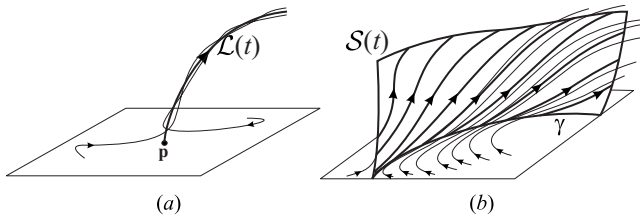


FIG. 1. (a) Separation curve $\mathcal{L}(t)$ emanating from a separation point \mathbf{p} . (b) Separation surface $\mathcal{S}(t)$ emanating from a separation line γ .

$$\left| \int_{t_0}^t \partial_z w(\mathbf{x}, 0, s) ds \right| < K, \quad (6)$$

$$\left| \int_{t_0}^t \nabla_x \partial_z w(\mathbf{x}, 0, s) ds \right| < K$$

for all t and for some constant $K > 0$. Note that for incompressible flows, we have

$$\partial_z w(\mathbf{x}, 0, t) \equiv 0$$

along the wall; thus Eq. (6) is always satisfied.

Our main assumption is that the velocity field \mathbf{v} has a steady asymptotic mean component

$$\bar{\mathbf{v}}(\mathbf{x}, z) = \lim_{T \rightarrow \infty} \frac{1}{T} \int_{t_0-T}^{t_0} \mathbf{v}(\mathbf{x}, z, t) dt, \quad (7)$$

bounded on the flow domain of interest for any choice of the initial time t_0 . Flows in this category include periodic and quasiperiodic flows, as well as turbulent flows with a steady mean component. These types of flows are sometimes referred to as stationary. To avoid ambiguity in terminology, we consider condition (7) as the precise definition of what we called “unsteady flow with a steady mean” in the Introduction.

Finally, we assume that the integrated velocity fluctuation

$$\Delta(\mathbf{x}, z, t) = \int_{t_0}^t [\mathbf{v}(\mathbf{x}, z, t) - \bar{\mathbf{v}}(\mathbf{x}, z)] dt \quad (8)$$

and its spatial derivatives up to third order are uniformly bounded in time on the flow domain of interest.

III. SEPARATION AND ATTACHMENT DEFINITIONS

Following Surana *et al.*,¹ we define flow separation as material ejection from the boundary due to the presence of distinguished material lines or material surfaces. Specifically, we say that fixed unsteady separation takes place along the boundary $z=0$ if fluid particles near the boundary converge to a time-dependent material line $\mathcal{L}(t)$ or a time-dependent material surface $\mathcal{S}(t)$, along which they are ejected from the boundary. In the language of dynamical systems, $\mathcal{L}(t)$ is a one-dimensional unstable manifold (separation curve) of a boundary point (*separation point*); $\mathcal{S}(t)$ is a two-dimensional unstable manifold (separation surface) of a curve of boundary points (*separation line*), as shown in Fig. 1.

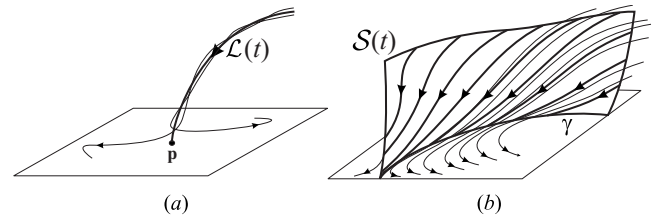


FIG. 2. (a) Attachment curve $\mathcal{L}(t)$ emanating from an attachment point \mathbf{p} . (b) Attachment surface $\mathcal{S}(t)$ emanating from an attachment line γ .

Note that while $\mathcal{L}(t)$ and $\mathcal{S}(t)$ will generally deform in time, their intersections with the boundary (\mathbf{p} and γ) remain fixed because of the no-slip boundary conditions (hence the term *fixed* unsteady separation). As we shall see below, this is the typical type of separation in flows that have a steady mean.

As in the steady case discussed by Surana *et al.*,¹ we only consider separation curves and surfaces that are *unique*, *bounded*, *smooth*, and *robust* with respect to flow perturbations (see Surana *et al.*¹ for a discussion of these properties). Also, following Surana *et al.*,¹ we define fixed unsteady attachment as fixed unsteady separation exhibited by the flow in backward time (see Fig. 2). This definition leads to the notion of an *attachment curve* (one-dimensional stable manifold) emanating from an *attachment point* \mathbf{p} and an *attachment surface* (two-dimensional stable manifold) emanating from an *attachment line* γ .

We stress two points related to our description of separation. First, our approach does not distinguish between small scale recirculation and large scale boundary-layer separation: Both involve material ejection from the boundary, but take place on different scales.

Second, the thin smoke and dye spikes commonly observed in flow visualization confirm that separation indeed takes place along unstable manifolds as we assume here. The question, however, remains: Do these observed spikes (manifolds) emanate directly from the wall or from nearby off-wall locations.

Based on available flow visualization results, we argue that the spikes typically form along wall-based unstable manifolds. Such wall-based manifolds have footprints in the wall-shear field that are commonly observed in numerical and laboratory experiments on boundary-layer separation.^{4,5,19} In steady flow over an infinite moving boundary²⁰ or around a rotating cylinder,²¹ however, Lagrangian separation appears to originate off the boundary. Such off-boundary separation, if indeed exists in physical flow, is not amenable to the boundary-based invariant manifold approach taken here, but can be captured by other methods.²²

IV. WEAKLY UNSTEADY PARTICLE DYNAMICS NEAR THE BOUNDARY

In this section, we show that the flow near the boundary is very close to the flow generated by an appropriately scaled and averaged version of the velocity \mathbf{v} . We first recall that fluid particles satisfy the 3D kinematic equations of motion,

$$\begin{aligned}\dot{x} &= u(x, y, z, t), \\ \dot{y} &= v(x, y, z, t), \\ \dot{z} &= w(x, y, z, t),\end{aligned}\quad (9)$$

or briefly,

$$\dot{\mathbf{x}} = \mathbf{u}(\mathbf{x}, z, t), \quad \dot{z} = w(\mathbf{x}, z, t).$$

Using the no-slip boundary conditions (2), Eq. (9) can be rewritten as

$$\begin{aligned}\dot{\mathbf{x}} &= z\mathbf{A}(\mathbf{x}, z, t), \\ \dot{z} &= zB(\mathbf{x}, z, t),\end{aligned}\quad (10)$$

where

$$\begin{aligned}\mathbf{A}(\mathbf{x}, z, t) &= \int_0^1 \partial_z \mathbf{u}(\mathbf{x}, sz, t) ds, \\ B(\mathbf{x}, z, t) &= \int_0^1 \partial_z w(\mathbf{x}, sz, t) ds.\end{aligned}\quad (11)$$

Equation (10) is a preliminary normal form for the flow; we shall further refine this normal form below.

Note that for incompressible flows, we have

$$\nabla_{\mathbf{x}} \cdot \mathbf{u} + \partial_z w = 0, \quad (12)$$

which implies $B(\mathbf{x}, 0, t) \equiv 0$ in Eq. (10) by the boundary conditions (2). Thus, in the incompressible case, Eq. (10) becomes

$$\dot{\mathbf{x}} = z\mathbf{A}(\mathbf{x}, z, t), \quad \dot{z} = z^2 C(\mathbf{x}, z, t), \quad (13)$$

with

$$C(\mathbf{x}, z, t) = \int_0^1 \int_0^1 \partial_z^2 w(\mathbf{x}, spz, t) p \, dp \, ds. \quad (14)$$

A. Locally incompressible normal form

It turns out that compressible particle motion can also be transformed to the form (13) by letting

$$z = \tilde{z} e^{\int_{t_0}^t \partial_z w(\mathbf{x}, 0, \tau) d\tau}. \quad (15)$$

Indeed, under this transformation, the equations of motion become

$$\dot{\mathbf{x}} = \tilde{z}\mathbf{A}_1(\mathbf{x}, \tilde{z}, t), \quad \dot{\tilde{z}} = \tilde{z}^2 C_1(\mathbf{x}, \tilde{z}, t), \quad (16)$$

where

$$\begin{aligned}\mathbf{A}_1(\mathbf{x}, \tilde{z}, t) &= e^{\int_{t_0}^t \partial_z w(\mathbf{x}, 0, \tau) d\tau} \mathbf{A}[\mathbf{x}, \tilde{z} e^{\int_{t_0}^t \partial_z w(\mathbf{x}, 0, \tau) d\tau}, t], \\ C_1(\mathbf{x}, \tilde{z}, t) &= e^{\int_{t_0}^t B(\mathbf{x}, 0, \tau) d\tau} \partial_z B(\mathbf{x}, 0, t) + O(\tilde{z}) \\ &= \frac{1}{2} e^{\int_{t_0}^t \partial_z w(\mathbf{x}, 0, \tau) d\tau} \partial_z^2 w(\mathbf{x}, 0, t) + O(\tilde{z}).\end{aligned}$$

B. First-order averaged normal form

To focus on the dynamics near the $z=0$ boundary, we apply the rescaling $\tilde{z} = \epsilon \bar{z}$ with $0 < \epsilon \ll 1$, which transforms the particle equations of motion (16) further to

$$\dot{\boldsymbol{\eta}} = \epsilon \mathbf{f}(\boldsymbol{\eta}, t) + \epsilon^2 \mathbf{g}(\boldsymbol{\eta}, t; \epsilon), \quad (17)$$

where $\boldsymbol{\eta} = (\mathbf{x}, \bar{z})^T$ and

$$\begin{aligned}\mathbf{f} &= \begin{pmatrix} \bar{z}\mathbf{A}_1(\mathbf{x}, 0, t) \\ \bar{z}^2 C_1(\mathbf{x}, 0, t) \end{pmatrix}, \\ \mathbf{g} &= \begin{pmatrix} \bar{z}^2 [\partial_z \mathbf{A}_1(\mathbf{x}, 0, t) + \mathcal{O}(\bar{z}\epsilon)] \\ \bar{z}^3 [\partial_z C_1(\mathbf{x}, 0, t) + \mathcal{O}(\bar{z}\epsilon)] \end{pmatrix}.\end{aligned}$$

For small $\epsilon > 0$, Eq. (17) is a slowly varying system to which the principle of averaging is applicable. More specifically, as we show in Appendix A, there exists a change in coordinates (averaging transformation),

$$\boldsymbol{\eta} = \boldsymbol{\zeta} + \epsilon \mathbf{w}(\boldsymbol{\zeta}, t), \quad (18)$$

$$\mathbf{w}(\boldsymbol{\zeta}, t) = \int_{t_0}^t [\mathbf{f}(\boldsymbol{\zeta}, \tau) - \bar{\mathbf{f}}(\boldsymbol{\zeta})] d\tau,$$

under which Eq. (17) becomes

$$\dot{\boldsymbol{\zeta}} = \epsilon \bar{\mathbf{f}}(\boldsymbol{\zeta}) + \epsilon^2 \mathbf{f}^1(\boldsymbol{\zeta}, t) + \mathcal{O}(\epsilon^3), \quad (19)$$

with

$$\bar{\mathbf{f}}(\boldsymbol{\zeta}) = \lim_{T \rightarrow \infty} \frac{1}{T} \int_{t_0-T}^{t_0} \mathbf{f}(\boldsymbol{\zeta}, \tau) d\tau,$$

$$\mathbf{f}^1(\boldsymbol{\zeta}, t) = \nabla_{\boldsymbol{\zeta}} \mathbf{f}(\boldsymbol{\zeta}, t) \mathbf{w}(\boldsymbol{\zeta}, t) + \mathbf{g}(\boldsymbol{\zeta}, t; 0) - \nabla_{\boldsymbol{\zeta}} \mathbf{w}(\boldsymbol{\zeta}, t) \bar{\mathbf{f}}(\boldsymbol{\zeta}).$$

Note that explicit time dependence now only appears in the $\mathcal{O}(\epsilon^2)$ terms of Eq. (19). Near the wall, therefore, the flow remains $\mathcal{O}(\epsilon^2)$ close to its steady mean when viewed in the $\boldsymbol{\zeta}$ coordinates.

C. Second-order averaged normal form

Our final change in variables pushes the explicit time dependence in Eq. (19) to even higher order. Namely, the second-order averaging transformation

$$\boldsymbol{\zeta} = \boldsymbol{\xi} + \epsilon^2 \mathbf{h}(\boldsymbol{\xi}, t), \quad (20)$$

$$\mathbf{h}(\boldsymbol{\xi}, t) = \int_{t_0}^t [\mathbf{f}^1(\boldsymbol{\xi}, \tau) - \bar{\mathbf{f}}^1(\boldsymbol{\xi})] d\tau$$

puts Eq. (19) in the form

$$\dot{\boldsymbol{\xi}} = \epsilon \bar{\mathbf{f}}(\boldsymbol{\xi}) + \epsilon^2 \bar{\mathbf{f}}^1(\boldsymbol{\xi}) + \mathcal{O}(\epsilon^3), \quad (21)$$

where

$$\bar{\mathbf{f}}^1(\boldsymbol{\xi}) = \lim_{T \rightarrow \infty} \frac{1}{T} \int_{t_0-T}^{t_0} \mathbf{f}^1(\boldsymbol{\xi}, \tau) d\tau, \quad (22)$$

and only the $\mathcal{O}(\epsilon^3)$ terms in Eq. (21) have explicit time dependence.

V. FIXED UNSTEADY SEPARATION AND ATTACHMENT CRITERIA

We shall first use the leading-order steady part of the second-order averaged normal form (21) to locate separation and attachment. This can be done based on the results of Surana *et al.*¹ on steady 3D separation. We then show that these steady separation and attachment locations persist if we take the additional $\mathcal{O}(\epsilon^3)$ unsteady terms into account in Eq. (21). We also obtain leading-order approximations for the time-varying off-wall part of the separation curves and surfaces. The mathematical details of our arguments are relegated to Appendices B and D; here we simply summarize the results.

A. Steady separation at leading order

The first-order-averaged normal form (19) shows that an unsteady compressible flow near a no-slip boundary can be viewed as a small perturbation to the steady velocity field,

$$\mathbf{v}^0(\mathbf{x}, \bar{z}) = [\epsilon \bar{z} \bar{\boldsymbol{\tau}}(\mathbf{x}), \epsilon \bar{z}^2 \bar{C}(\mathbf{x})], \quad (23)$$

where the weighted average of the wall shear,

$$\bar{\boldsymbol{\tau}}(\mathbf{x}) = \lim_{T \rightarrow \infty} \frac{1}{T} \int_{t_0-T}^{t_0} e^{\int_{t_0}^{\tau} \partial_z w(\mathbf{x}, 0, s) ds} \partial_z \mathbf{u}(\mathbf{x}, 0, \tau) d\tau, \quad (24)$$

is obtained from the instantaneous wall shear,

$$\boldsymbol{\tau}(\mathbf{x}, t) = \partial_z \mathbf{u}(\mathbf{x}, 0, t). \quad (25)$$

Furthermore, the constant \bar{C} in Eq. (23) is defined as

$$\bar{C}(\mathbf{x}) = \frac{1}{2} \lim_{T \rightarrow \infty} \frac{1}{T} \int_{t_0-T}^{t_0} e^{\int_{t_0}^{\tau} \partial_z w(\mathbf{x}, 0, s) ds} \partial_z^2 w(\mathbf{x}, 0, \tau) d\tau, \quad (26)$$

measuring the weighted average rate of stretching normal to the boundary.

The particle equations of motion for the velocity field (23) are given by

$$\dot{\mathbf{x}} = \epsilon \bar{z} \bar{\boldsymbol{\tau}}(\mathbf{x}), \quad (27)$$

$$\dot{\bar{z}} = \epsilon \bar{z}^2 \bar{C}(\mathbf{x}).$$

As in Surana *et al.*,¹ we introduce the rescaled time variable,

$$s = \epsilon \int_{t_0}^t \bar{z}(r) dr, \quad (28)$$

so that the above equations of motion become

$$\mathbf{x}' = \bar{\boldsymbol{\tau}}(\mathbf{x}), \quad (29)$$

$$\bar{z}' = \bar{z} \bar{C}(\mathbf{x}),$$

with prime denoting differentiation with respect to the rescaled time s .

In the rescaled system (29), the averaged wall shear generates a fictitious flow,

$$\mathbf{x}' = \bar{\boldsymbol{\tau}}(\mathbf{x}), \quad (30)$$

on the $z=0$ boundary. We refer to a trajectory $\mathbf{x}(s, \mathbf{x}_0)$ of Eq.

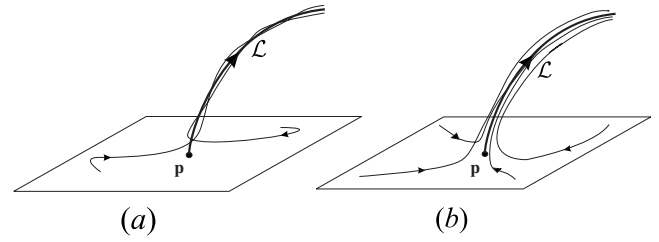


FIG. 3. Different types of separation points and the associated separation curves in the steady averaged limit (23): (a) stable foci and (b) stable node. Under conditions of Theorem 1, time-dependent perturbations of these separation curves continue to act as unstable manifolds for \mathbf{p} in the original velocity field \mathbf{v} .

(30) starting from \mathbf{x}_0 at $s=0$ as an *averaged wall-shear trajectory*. A connected union of wall-shear trajectories will be called an *averaged wall-shear line*, denoted by γ .

As shown by Surana *et al.*,¹ steady separation locations crucially depend on the rate at which wall-shear trajectories converge to, or diverge from, each other. In the context of the rescaled averaged flow (30), these rates are measured by the averaged normal strain rate field,

$$\bar{S}_{\perp}(\mathbf{x}) = \frac{\bar{\boldsymbol{\omega}} \cdot ([\nabla_{\mathbf{x}} \bar{\boldsymbol{\tau}}] \bar{\boldsymbol{\omega}})}{|\bar{\boldsymbol{\omega}}|^2} \Big|_{\mathbf{x}},$$

where $\nabla_{\mathbf{x}} \bar{\boldsymbol{\tau}}(\mathbf{x})$ is the wall-tangential gradient of $\bar{\boldsymbol{\tau}}(\mathbf{x})$ and $\bar{\boldsymbol{\omega}}$ is the averaged on-wall vorticity field,

$$\bar{\boldsymbol{\omega}}(\mathbf{x}) = \bar{\boldsymbol{\tau}}^{\perp}(\mathbf{x}), \quad (31)$$

with the notation $(a, b)^{\perp} = (-b, a)$.

With the above quantities at hand, we can apply the results of Surana *et al.*¹ to locate separation and attachment in the steady averaged velocity field $\mathbf{v}^0(\mathbf{x}, \bar{z})$. Figure 3 shows the two possible types of separation points \mathbf{p} that $\mathbf{v}^0(\mathbf{x}, \bar{z})$ may admit; Fig. 4 illustrates the four basic types of separation lines γ that can occur in $\mathbf{v}^0(\mathbf{x}, \bar{z})$.

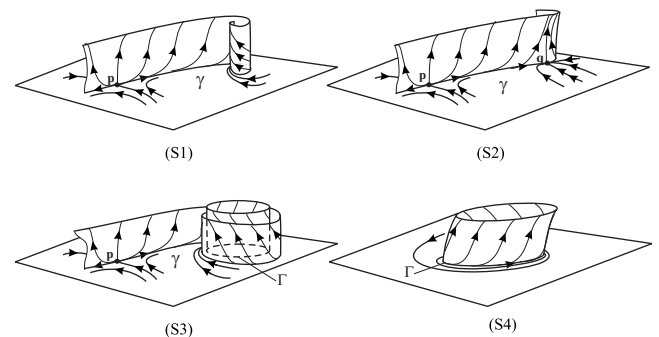


FIG. 4. The four basic separation lines and associated separation surfaces in the averaged steady limit (23). Under conditions of Theorem 2, time-dependent perturbations of the separation surface continue to act as unstable manifolds of γ in the full velocity field \mathbf{v} .

B. Criteria for fixed separation and attachment points in the unsteady flow

As a second step, we shall use techniques from nonlinear dynamical system theory to show that the above steady separation structures have nearby time-dependent counterparts in the original unsteady velocity field \mathbf{v} . We list the final results below and relegate their detailed proof to Appendix B.

Theorem 1: Suppose that a point \mathbf{p} satisfies

$$\bar{\tau}(\mathbf{p}) = 0, \quad \nabla_{\mathbf{x}} \cdot \bar{\tau}(\mathbf{p}) < 0, \quad (32)$$

$$\det \nabla_{\mathbf{x}} \bar{\tau}(\mathbf{p}) > 0, \quad \bar{C}(\mathbf{p}) > 0.$$

Then $(\mathbf{x}, z) = (\mathbf{p}, 0)$ is a fixed unsteady separation point for the velocity field \mathbf{v} .

By reversing time in the proof of Theorem 1, we find that if

$$\bar{\tau}(\mathbf{p}) = 0, \quad \nabla_{\mathbf{x}} \cdot \bar{\tau}(\mathbf{p}) > 0, \quad (33)$$

$$\det \nabla_{\mathbf{x}} \bar{\tau}(\mathbf{p}) > 0, \quad \bar{C}(\mathbf{p}) < 0,$$

are satisfied, then \mathbf{p} is a fixed attachment point.

In summary, we have the following results for the original unsteady velocity field \mathbf{v} :

- (S0) A separation point $(\mathbf{p}, 0)$ on the $z=0$ boundary is either a stable node or a stable spiral of the time-averaged wall-shear field (24) with $\bar{C}(\mathbf{p}) > 0$.
- (R0) An attachment point $(\mathbf{p}, 0)$ on the $z=0$ boundary is either an unstable node or unstable spiral of the time-averaged wall-shear field (24) with $\bar{C}(\mathbf{p}) < 0$.

C. Criteria for fixed separation and attachment lines in the unsteady flow

We now list our main result for fixed separation lines for the velocity field \mathbf{v} ; we prove these results in Appendix B.

Theorem 2: Let γ be a bounded wall-shear line of the time averaged wall-shear field (24). Assume that at each point \mathbf{x} of γ , we have

$$\bar{S}_{\perp}(\mathbf{x}) - \bar{C}(\mathbf{x}) < 0, \quad \bar{C}(\mathbf{x}) > 0. \quad (34)$$

Assume further that one of the following holds:

- (S1) γ originates from a saddle \mathbf{p} and ends at a stable spiral \mathbf{q} .
- (S2) γ originates from a saddle \mathbf{p} and ends at a stable node \mathbf{q} . Also, γ is tangent to the direction of weaker attraction at \mathbf{q} .
- (S3) γ originates from a saddle \mathbf{p} and spirals onto a stable limit cycle Γ .
- (S4) γ is a stable limit cycle Γ .

Then γ is a fixed separation line for the unsteady velocity field \mathbf{v} .

We prove Theorem 1 in Appendix B 1. By reversing time in the proof, we obtain a criterion for attachment lines.

Specifically, let γ be a bounded wall-shear line of the time-averaged wall-shear field (24). Assume that at each point \mathbf{x} of γ , we have

$$\bar{S}_{\perp}(\mathbf{x}) - \bar{C}(\mathbf{x}) > 0, \quad \bar{C}(\mathbf{x}) < 0. \quad (35)$$

Assume further that one of the following holds:

- (R1) γ originates from an unstable spiral \mathbf{p} and ends at a saddle \mathbf{q} .
- (R2) γ originates from a unstable node \mathbf{p} and ends at a saddle \mathbf{q} . Also, γ is tangent to direction of weaker repulsion at \mathbf{p} .
- (R3) γ spirals off an unstable limit cycle Γ and ends at a saddle \mathbf{q} .
- (R4) γ is a unstable limit cycle Γ .

Then γ is a fixed attachment line for the unsteady velocity field \mathbf{v} .

The time-averaged wall-shear zeros \mathbf{p} and \mathbf{q} , as well as the limit cycle Γ featured above, must be nondegenerate: they must attract or repel nearby time averaged wall-shear trajectories exponentially in the rescaled time s (28). For the details of these nondegeneracy conditions, we refer to Surana *et al.*¹

D. Fixed unsteady separation at corners

The above nondegeneracy conditions always fail at the intersection of the wall with another vertical boundary. Since one of the examples considered in this paper involves such a situation, we briefly outline below how the above conditions must be modified to apply in this degenerate case.

Consider, for simplicity, two no-slip boundaries given by $x=0$ and $z=0$, intersecting in a corner that is just the y axis itself. As we show in Appendix C, the steady averaged normal form in this case takes the form

$$\begin{aligned} \dot{\bar{x}} &= \bar{x}^2 \bar{\tau}_1(\bar{x}, y), \\ \dot{y} &= \bar{x} \bar{z} \bar{\tau}_2(\bar{x}, y), \end{aligned} \quad (36)$$

$$\dot{\bar{z}} = \bar{x} \bar{z}^2 \bar{\tau}_3(\bar{x}, y),$$

where

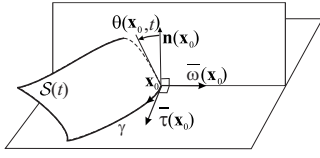
$$\bar{\tau}_1(\bar{x}, y) = \lim_{T \rightarrow \infty} \frac{1}{T} \int_{t_0-T}^{t_0} e^{\int_{t_0}^t \bar{C}(\bar{x}, y, 0, \tau) d\tau} \partial_{\bar{x}\bar{x}\bar{z}}^3 u(0, y, 0, t) dt,$$

$$\bar{\tau}_2(\bar{x}, y) = \lim_{T \rightarrow \infty} \frac{1}{T} \int_{t_0-T}^{t_0} e^{\int_{t_0}^t \bar{C}(\bar{x}, y, 0, \tau) d\tau} \partial_{\bar{x}\bar{z}}^2 v(0, y, 0, t) dt,$$

$$\bar{\tau}_3(\bar{x}, y) = \lim_{T \rightarrow \infty} \frac{1}{T} \int_{t_0-T}^{t_0} e^{\int_{t_0}^t \bar{C}(\bar{x}, y, 0, \tau) d\tau} \partial_{\bar{x}\bar{z}\bar{z}}^3 w(0, y, 0, t) dt.$$

With this notation, the wall-shear field $\bar{\tau}$ (24) can be written as

$$\bar{\tau} = (\bar{x}^2 \bar{\tau}_1, \bar{x} \bar{\tau}_2). \quad (37)$$

FIG. 5. Definition of the separation angle $\theta(\mathbf{x}_0, t)$.

Let γ be an averaged wall-shear trajectory of Eq. (37) that terminates in a point $\mathbf{p} = (0, p)$ of the $y=0$ corner of the $z=0$ plane. Based on the analysis of Surana *et al.*,¹ we conclude the following:

(Sc1) \mathbf{p} satisfies

$$\bar{\tau}_2(\mathbf{p}) = 0,$$

and can only be either a saddle or a node of the $\bar{\tau}$ vector field.

(Sc2) \mathbf{p} is a nondegenerate node within the $z=0$ plane if

$$[\bar{\tau}_1(\mathbf{p}) + \partial_y \bar{\tau}_2(\mathbf{p})]^2 > 4\bar{\tau}_1(\mathbf{p})\partial_y \bar{\tau}_2(\mathbf{p}) > 0, \quad (38)$$

whereas \mathbf{p} is a nondegenerate saddle within the $z=0$ plane if

$$\bar{\tau}_1(\mathbf{p})\partial_y \bar{\tau}_2(\mathbf{p}) < 0. \quad (39)$$

(Sc3) For separation to take place along γ , the leading-order stretching rate off the $z=0$ plane at the point \mathbf{p} must satisfy

$$\bar{\tau}_3(\mathbf{p}) > 0,$$

and we must also have

$$\bar{S}_\perp(\mathbf{x}) - \bar{C}(\mathbf{x}) < 0, \quad \bar{C}(\mathbf{x}) > 0, \quad (40)$$

for all points $\mathbf{x} \neq \mathbf{p}$ of γ .

E. Separation- and attachment-slope formulas

A separation curve $\mathcal{L}(t)$ is a time-dependent material line emanating from the separation point \mathbf{p} , it can locally be represented as

$$\mathbf{x} = \mathbf{p} + z\mathbf{g}_0(t) + \mathcal{O}(z^2),$$

where $\mathbf{g}_0(t)$ denotes the time-dependent slope of $\mathcal{L}(t)$.

For a separation surface $\mathcal{S}(t)$ emanating from a fixed separation line γ , we define the separation angle $\theta(\mathbf{x}_0, t)$ at a point \mathbf{x}_0 of γ as follows: $\theta(\mathbf{x}_0, t)$ is the angle between the wall normal and the tangent of $\mathcal{S}(t)$ at \mathbf{x}_0 (see Fig. 5).

If we use the first-order averaged normal form (19) to compute $\mathbf{g}_0(t)$ or $\theta(\mathbf{x}_0, t)$, we always obtain zero values for

both. We can, however, use the second-order averaged normal form (21) to obtain a more refined approximation for the separation slope. Specifically, as we show in Appendix D, we obtain that at time t_0 , the slope of a separation curve emanating from \mathbf{p} is given by

$$\mathbf{g}_0(t_0) = -[\bar{\mathbf{P}}(\mathbf{p})]^{-1}\bar{\mathbf{Q}}(\mathbf{p}), \quad (41)$$

where

$$\bar{\mathbf{P}}(\mathbf{x}) = \lim_{T \rightarrow \infty} \frac{1}{T} \int_{t_0-T}^{t_0} \mathbf{P}(\mathbf{x}, \tau, t_0) d\tau,$$

$$\bar{\mathbf{Q}}(\mathbf{x}) = \lim_{T \rightarrow \infty} \frac{1}{T} \int_{t_0-T}^{t_0} \mathbf{Q}(\mathbf{x}, \tau, t_0), \quad (42)$$

with

$$\begin{aligned} \mathbf{P}(\mathbf{x}, \tau, t_0) = & e^{\int_{t_0}^{\tau} \partial_z w(\mathbf{x}, 0, s) ds} \left\{ \nabla_{\mathbf{x}} \partial_z \mathbf{u}(\mathbf{x}, 0, \tau) + \partial_z \mathbf{u}(\mathbf{x}, 0, \tau) \right. \\ & \left. \times \left[\int_{t_0}^{\tau} \nabla_{\mathbf{x}} \partial_z w(\mathbf{x}, 0, s) ds \right]^T \right\} \\ & - \frac{1}{2} e^{\int_{t_0}^{\tau} \partial_z w(\mathbf{x}, 0, s) ds} \mathbf{I} \partial_z^2 w(\mathbf{x}, 0, \tau), \end{aligned}$$

$$\begin{aligned} \mathbf{Q}(\mathbf{x}, \tau, t_0) = & \frac{1}{2} e^{2 \int_{t_0}^{\tau} \partial_z w(\mathbf{x}, 0, s) ds} \partial_z^2 \mathbf{u}(\mathbf{x}, 0, \tau) \\ & + \mathbf{P}(\mathbf{x}, \tau, t_0) \int_{t_0}^{\tau} e^{\int_{t_0}^p \partial_z w(\mathbf{x}, 0, s) ds} \partial_z \mathbf{u}(\mathbf{x}, 0, p) dp. \end{aligned}$$

The above slope formula is equally valid for attachment curves by a time-reversal argument.

We also show in Appendix D that at time t_0 , the slope of a separation surface at a boundary point \mathbf{x}_0 satisfies

$$\tan[\theta(\mathbf{x}_0, t_0)] = \int_{-\infty}^0 E(q) \frac{\bar{\mathbf{R}} \cdot \bar{\boldsymbol{\omega}}}{|\bar{\boldsymbol{\omega}}|} \Big|_{\mathbf{x}=\mathbf{x}(q, \mathbf{x}_0)} dq, \quad (43)$$

where

$$E(q) = e^{\int_0^q [\bar{C}[\mathbf{x}(r, \mathbf{x}_0)] - \bar{S}_\perp(r)] dr}, \quad (44)$$

and $\mathbf{x}(q, \mathbf{x}_0)$ is a trajectory on the separation line γ satisfying the differential equation (30). Furthermore, the function $\bar{\mathbf{R}}$ in the formula (43) is defined as

$$\bar{\mathbf{R}}(\mathbf{x}, t_0) = \lim_{T \rightarrow \infty} \frac{1}{T} \int_{t_0-T}^{t_0} \mathbf{R}(\mathbf{x}, \tau, t_0) d\tau,$$

where

$$\begin{aligned} \mathbf{R}(\mathbf{x}, \tau, t_0) = & \frac{1}{2} e^{2 \int_{t_0}^{\tau} \partial_z w(\mathbf{x}, 0, s) ds} \partial_z^2 \mathbf{u}(\mathbf{x}, 0, \tau) + \mathbf{P}(\mathbf{x}, \tau, t_0) \int_{t_0}^{\tau} \left[e^{\int_{t_0}^p \partial_z w(\mathbf{x}, 0, s) ds} \partial_z \mathbf{u}(\mathbf{x}, 0, p) - \bar{\tau}(\mathbf{x}) \right] dp \\ & + \left\{ \int_{t_0}^{\tau} \left[e^{\int_{t_0}^p \partial_z w(\mathbf{x}, 0, s) ds} \left[\nabla_{\mathbf{x}} \partial_z \mathbf{u}(\mathbf{x}, 0, p) + \partial_z \mathbf{u}(\mathbf{x}, 0, p) \left[\int_{t_0}^p \nabla_{\mathbf{x}} \partial_z w(\mathbf{x}, 0, s) ds \right]^T \right] - \nabla_{\mathbf{x}} \bar{\tau}(\mathbf{x}) \right] dp \right\} \bar{\tau}(\mathbf{x}). \end{aligned}$$

Attachment slopes obey a similar formula with the limit in the improper integral taken in forward time,

$$\tan(\theta(\mathbf{x}_0, t_0)) = - \int_0^{+\infty} E(q) \frac{\bar{\mathbf{R}} \cdot \bar{\boldsymbol{\omega}}}{|\bar{\boldsymbol{\omega}}|} \Big|_{\mathbf{x}=\mathbf{x}(q, \mathbf{x}_0)} dq. \quad (45)$$

Note that the computation of above separation/attachment criteria requires the knowledge of various wall normal derivatives, which may be difficult to obtain directly in experiments. By definition, the $\partial_z \mathbf{u}(\mathbf{x}, 0, t)$ is related to time-dependent wall-shear stress $\boldsymbol{\tau}_s$ as

$$\partial_z \mathbf{u}(\mathbf{x}, 0, t) = \boldsymbol{\tau}(\mathbf{x}, t) = \frac{1}{\mu} \boldsymbol{\tau}_s(\mathbf{x}, t), \quad (46)$$

where μ is the dynamic viscosity of the fluid. Restriction of continuity equation on the wall [Eq. (4)] leads to

$$e^{-\int_{t_0}^t \partial_z w(\mathbf{x}, 0, s) ds} = \frac{\rho(\mathbf{x}, 0, t)}{\rho(\mathbf{x}, 0, t_0)}, \quad (47)$$

while restriction of the Navier–Stokes equation yields

$$\partial_z^2 u(\mathbf{x}, 0, t) = \frac{1}{\mu} \nabla_x p(\mathbf{x}, 0, t).$$

Hence, $\partial_z w(\mathbf{x}, 0, t)$ and $\partial_z^2 u(\mathbf{x}, 0, t)$ can be obtained from on wall measurements of density and pressure. For incompressible flows, we have $\partial_z w(\mathbf{x}, 0, t) \equiv 0$ and

$$\partial_z^2 w(\mathbf{x}, 0, t) = -\nabla_x \cdot \boldsymbol{\tau}(\mathbf{x}, t). \quad (48)$$

Hence, for incompressible Navier–Stokes flows, the formulas (41), (43), and (45) can be expressed only in terms of the wall shear, the wall pressure, and their derivatives (see Surana *et al.*¹ for details).

F. Algorithm for locating separation and attachment

The above results lead to the following algorithm for locating separation and attachment in unsteady flows with a steady mean component (see Surana *et al.*²³ for details):

- (1) For the time averaged wall-shear field $\bar{\boldsymbol{\tau}}(\mathbf{x})$ [Eq. (24)], find all nondegenerate zeros \mathbf{p}_i and limit cycles Γ_j . The zeros and limit cycle should satisfy nondegeneracy condition, specifically, a nondegenerate node \mathbf{p} satisfies

$$[\nabla_x \cdot \bar{\boldsymbol{\tau}}(\mathbf{p})]^2 > 4 \det \nabla_x \bar{\boldsymbol{\tau}}(\mathbf{p}) > 0, \quad (49)$$

a nondegenerate saddle \mathbf{p} satisfies

$$\det \nabla_x \bar{\boldsymbol{\tau}}(\mathbf{p}) < 0, \quad (50)$$

a nondegenerate spiral \mathbf{p} satisfies

$$0 < [\nabla_x \cdot \bar{\boldsymbol{\tau}}(\mathbf{p})]^2 < 4 \det \nabla_x \bar{\boldsymbol{\tau}}(\mathbf{p}), \quad (51)$$

and a nondegenerate limit cycle Γ satisfies

$$\int_{\Gamma} \frac{\bar{\boldsymbol{\omega}} \cdot (\nabla_x \bar{\boldsymbol{\tau}} \bar{\boldsymbol{\omega}})}{|\bar{\boldsymbol{\omega}}|^2} \Big|_{\mathbf{x}=\mathbf{x}(s, \mathbf{x}_0)} ds \neq 0. \quad (52)$$

- (2) For each nondegenerate wall-shear saddle \mathbf{p}_k , find its stable and unstable manifolds in the $z=0$ plane. The manifold $W^u(\mathbf{p}_k)$ is obtained numerically by advecting a small line segment—initially tangent to the unstable ei-

genvector of \mathbf{p}_k —using the flow of $\dot{\mathbf{x}}=\bar{\boldsymbol{\tau}}(\mathbf{x})$. In other words, we take an initial condition on the unstable eigenvector of \mathbf{p}_k sufficiently close to \mathbf{p}_k and solve the system $\dot{\mathbf{x}}=\bar{\boldsymbol{\tau}}(\mathbf{x})$ for that initial condition. The manifold $W^s(\mathbf{p}_k)$ is obtained by backward advecting a small line segment—initially tangent to the stable eigenvector of \mathbf{p} —using the flow of $\dot{\mathbf{x}}=\bar{\boldsymbol{\tau}}(\mathbf{x})$.

- (3) Identify separation and attachment points using the criteria (S0) and (R0).
- (4) Identify separation and attachment lines from the criteria (S1)–(S4) and (R1)–(R4). At corners, use (Sc1)–(Sc3) and its counterpart (Rc1)–(Rc3).
- (5) Compute the slope of separation and attachment curves at current time t_0 , using Eq. (41).
- (6) Compute first-order approximations at current time t_0 for attachment and separation surfaces from the angle formula in Eq. (43) or (45).

VI. AN ANALYTIC EXAMPLE: RANDOMLY VARYING SEPARATION BUBBLE

In this section, we analyze a randomized version of the steady incompressible separation bubble flow model studied by Surana *et al.*¹ The velocity field for this flow is given by

$$u = z \left[\left(\frac{x}{a} \right)^2 + \left(\frac{y}{b} \right)^2 - 1 \right] + z^2 \left[\alpha + \delta x + \left(\frac{c}{6} - \frac{2}{3a^2} - \frac{1}{3b^2} \right) z \right],$$

$$v = -yz[cx + d + \gamma r(t)] + z^2(\beta + \delta y), \quad (53)$$

$$w = \frac{d + \gamma r(t)}{2} z^2 + \left[\frac{c}{2} - \frac{1}{a^2} \right] x z^2 - \frac{2\delta}{3} z^3,$$

where $r(t)$ is a zero-mean random variable with normal distribution. This model is derived from the Navier–Stokes equations by using the perturbative procedure of Perry and Chong²⁴ and is dynamically consistent up to cubic order in the spatial variables near the no-slip boundary. Physically, the velocity field models the loss of stability of the steady separation bubble that develops random oscillations. As we show below, the separation pattern we identify in this flow is commonly observed over moving vehicles.²⁵

Because $r(t)$ has zero mean, its integral,

$$F(t) = F(t_0) + \int_{t_0}^t r(\tau) d\tau, \quad (54)$$

is bounded, leading to

$$\lim_{T \rightarrow \infty} \frac{1}{T} \int_{t_0-T}^{t_0} r(t) dt = 0. \quad (55)$$

Thus, the averaged velocity field is given by the $\gamma=0$ limit of Eq. (53), which is bounded on bounded sets. Also, the function

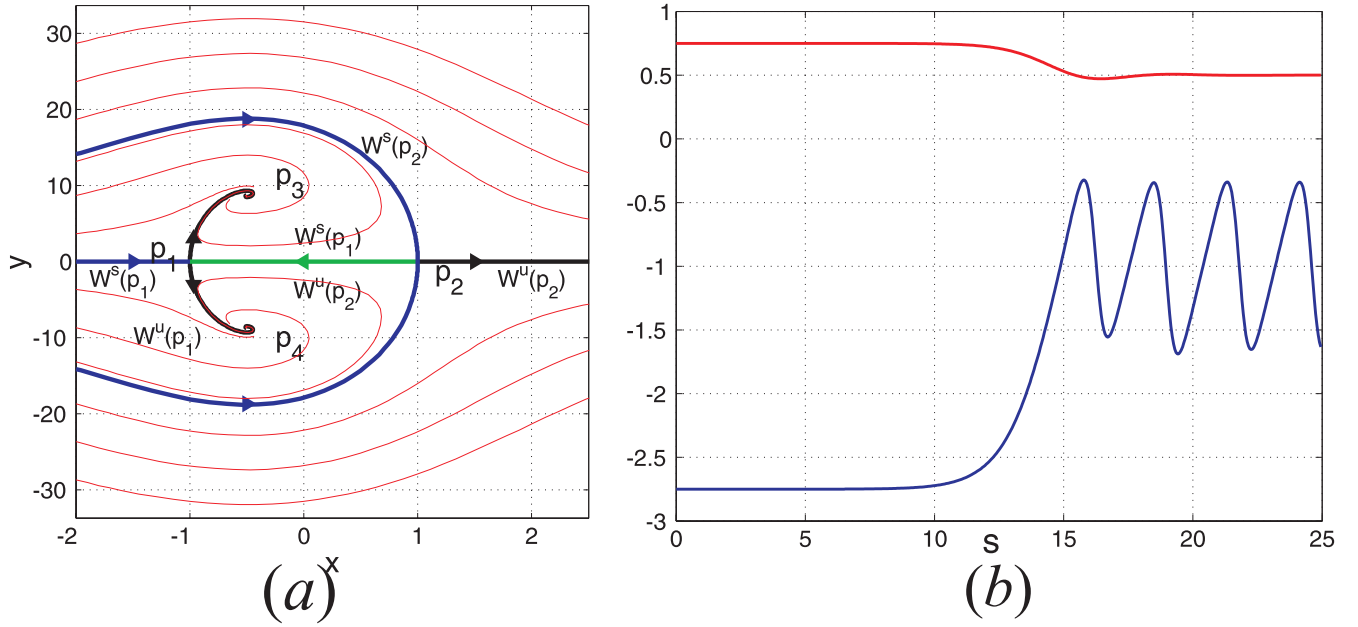


FIG. 6. (Color) (a) Averaged wall-shear field for random bubble flow with parameters $a=1$, $b=1$, $c=1$, $d=\frac{1}{2}$, $\alpha=1$, $\beta=0$, $\delta=1$, and $\gamma=5$. (b) The blue curve represents $\bar{S}_\perp[\mathbf{x}(s)] - \bar{C}[\mathbf{x}(s)]$ and the red one is $\bar{C}[\mathbf{x}(s)]$, where $\mathbf{x}(s)$ denotes the branch of $W^u(\mathbf{p}_1)$ connecting to \mathbf{p}_3 .

$$\Delta(\mathbf{x}, z, t) = \gamma F(t) \begin{pmatrix} 0 \\ -yz \\ z^2/2 \end{pmatrix}$$

and its spatial derivatives are bounded on bounded sets. All the assumptions of Sec. II are therefore satisfied.

We obtain the averaged wall-shear and vertical strain coefficient in the form

$$\bar{\boldsymbol{\tau}}(\mathbf{x}) = \begin{pmatrix} \frac{x^2}{a^2} + \frac{y^2}{b^2} - 1 \\ -ycx - yd \end{pmatrix}, \quad \bar{C}(\mathbf{x}) = \frac{d}{2} + \left(\frac{c}{2} - \frac{1}{a^2}\right)x. \quad (56)$$

With these quantities at hand, we can verify the following assertions:

(i) For $d < ac$, the vector field $\bar{\boldsymbol{\tau}}(\mathbf{x})$ admits four zeros,

$$\mathbf{p}_1 = \begin{pmatrix} -a \\ 0 \end{pmatrix}, \quad \mathbf{p}_2 = \begin{pmatrix} a \\ 0 \end{pmatrix},$$

$$\mathbf{p}_3 = \begin{bmatrix} -d/c \\ -b\sqrt{1 - \left(\frac{d}{ac}\right)^2} \end{bmatrix},$$

$$\mathbf{p}_4 = \begin{bmatrix} -d/c \\ b\sqrt{1 - \left(\frac{d}{ac}\right)^2} \end{bmatrix},$$

which can be classified as follows (cf. Surana *et al.*¹):

(1) \mathbf{p}_1 is a saddle, since $\det \nabla_{\mathbf{x}} \bar{\boldsymbol{\tau}}(\mathbf{p}_1) = 2a(d-ac) < 0$, with

$$\bar{C}(\mathbf{p}_1) = \frac{d-ac}{2} + \frac{1}{a}. \quad (57)$$

(2) \mathbf{p}_2 is also a saddle, as $\det \nabla_{\mathbf{x}} \bar{\boldsymbol{\tau}}(\mathbf{p}_2) = -2a(d+ac) < 0$, with

$$\bar{C}(\mathbf{p}_2) = \frac{d+ac}{2} - \frac{1}{a}. \quad (58)$$

(3) \mathbf{p}_3 and \mathbf{p}_4 are stable foci because

$$\det \nabla_{\mathbf{x}} \bar{\boldsymbol{\tau}}(\mathbf{p}_{3,4}) = \frac{2}{c} \left[1 - \left(\frac{d}{ac}\right)^2 \right] > 0,$$

$$\nabla_{\mathbf{x}} \cdot \bar{\boldsymbol{\tau}}(\mathbf{p}_{3,4}) = -\frac{2d}{ca^2} < 0, \quad (59)$$

$$\det \nabla_{\mathbf{x}} \bar{\boldsymbol{\tau}}(\mathbf{p}_{3,4}) > [\nabla_{\mathbf{x}} \cdot \bar{\boldsymbol{\tau}}(\mathbf{p}_{3,4})]^2/4$$

hold with

$$\bar{C}(\mathbf{p}_{3,4}) = \frac{d}{a^2c} > 0. \quad (60)$$

Therefore, by Theorem 1, \mathbf{p}_3 and \mathbf{p}_4 are separation points.

(ii) Based on the above inequalities, we conclude that the union of the two branches of the unstable manifold $W^u(\mathbf{p}_1)$ of the saddle \mathbf{p}_1 is a separation line candidate. Moreover, the two conditions in Eq. (34) are satisfied for this separation line, as shown in Fig. 6(b). Hence, by Theorem 2, fixed separation occurs along $W^u(\mathbf{p}_1)$.

The slopes of the separation profiles at the separation points \mathbf{p}_3 and \mathbf{p}_4 are now given by

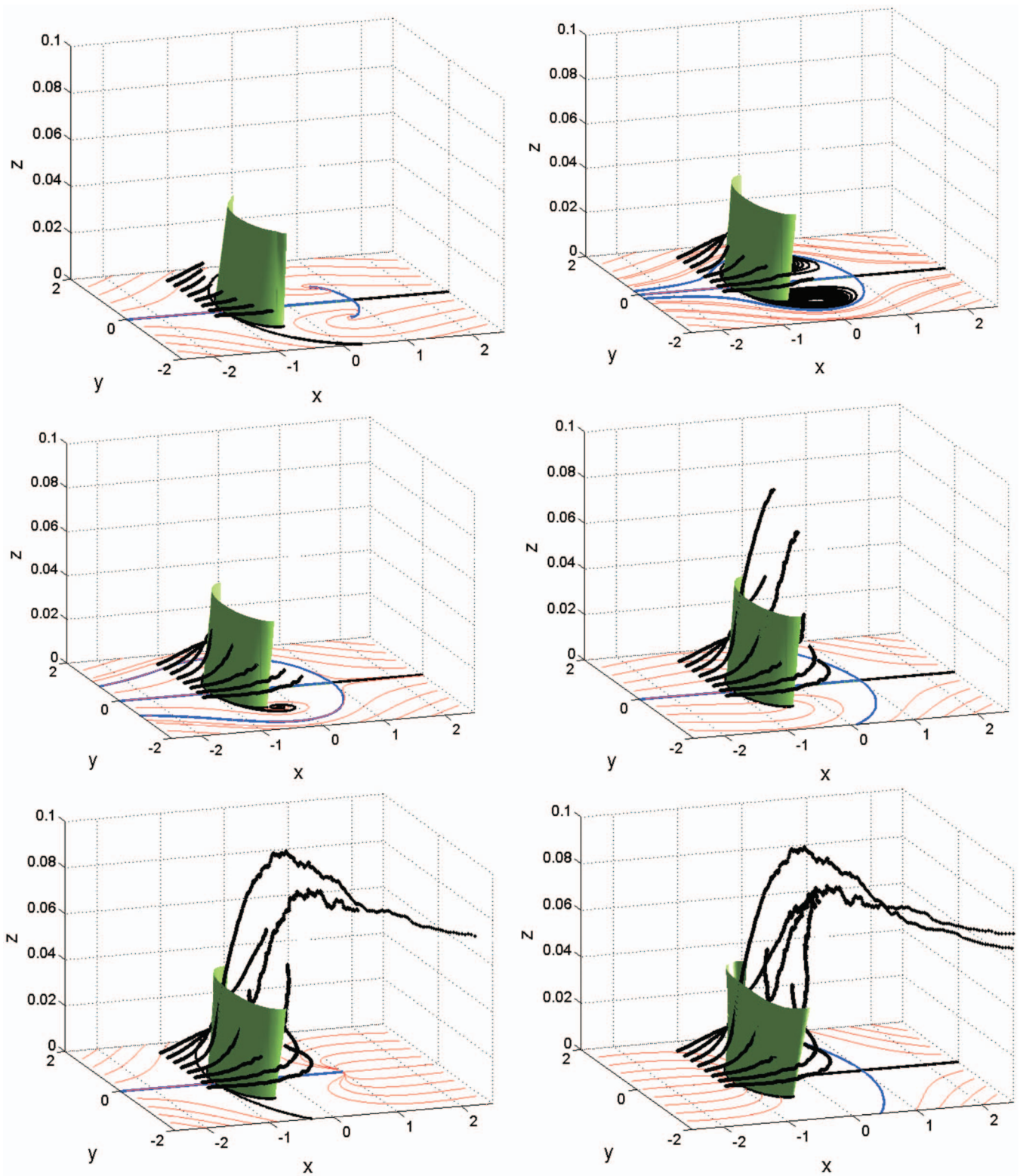


FIG. 7. (Color) Fixed separation exhibited by fluid particles in the random separation bubble flow. The pictures correspond to the increasing sequence of times $t=55, 103, 135, 185, 215,$ and 249 .

$$\mathbf{g}_0(\mathbf{p}_3, t) = - \begin{bmatrix} -\frac{3d}{ca^2} & -\frac{2}{b} \sqrt{1 - \left(\frac{d}{ac}\right)^2} \\ cb \sqrt{1 - \left(\frac{d}{ac}\right)^2} & -\frac{d}{ca^2} \end{bmatrix}^{-1} \times \left\{ \begin{pmatrix} \alpha \\ \beta \end{pmatrix} + \delta \mathbf{p}_3 + \gamma \begin{bmatrix} 2 \left(1 - \left(\frac{d}{ac}\right)^2\right) \\ \frac{bd}{ca^2} \sqrt{1 - \left(\frac{d}{ac}\right)^2} \end{bmatrix} F(t) \right\},$$

$$\mathbf{g}_0(\mathbf{p}_4, t) = - \begin{bmatrix} -\frac{3d}{ca^2} & \frac{2}{b} \sqrt{1 - \left(\frac{d}{ac}\right)^2} \\ -cb \sqrt{1 - \left(\frac{d}{ac}\right)^2} & -\frac{d}{ca^2} \end{bmatrix}^{-1} \times \left\{ \begin{pmatrix} \alpha \\ \beta \end{pmatrix} + \delta \mathbf{p}_4 + \gamma \begin{bmatrix} 2 \left(1 - \left(\frac{d}{ac}\right)^2\right) \\ -\frac{bd}{ca^2} \sqrt{1 - \left(\frac{d}{ac}\right)^2} \end{bmatrix} F(t) \right\},$$

respectively. The separation line in this example is the union of two branches of the unstable manifold $W^u(\mathbf{p}_1)$ of \mathbf{p}_1 . We compute the separation slope along $W^u(\mathbf{p}_1)$ numerically using formula (43).

In our numerical simulations of this model, we set the standard deviation of $r(t)$ equal to 0.2. We sampled $r(t)$ at multiples of $\Delta T=0.2$ and used a cubic spline interpolation to obtain velocity values in Eq. (53) for intermediate times. We show the corresponding numerical simulation of fluid particle motion in Fig. 7. Despite the drastic changes in the instantaneous wall-shear topology, the separation occurs at a fixed location along the separation surface predicted by our theory.

VII. TIME-PERIODIC LID-DRIVEN CAVITY FLOW

We now turn to the direct numerical simulation of a time-periodic lid-driven cavity, a classic benchmark problem with complex separation and attachment topologies.²³ Beyond their technological importance, cavity flows are of independent scientific interest as they display almost all 3D fluids phenomena in the simplest of geometrical settings.²⁶

The nondimensionalized computational model (Fig. 8) consists of a cube with sides $L=1$. The top wall in the z -direction is driven at a time-periodic velocity $U(t)=U_m+0.7 \sin t$ in the x -direction with a mean velocity $U_m=0.3$. The velocity distribution on the moving top wall is tapered to zero toward the sides according to a parabolic profile; this is to avoid velocity singularities at these locations. For details of the numerical methodology used in our simulation, we refer the reader to Surana *et al.*,²³ where the same cavity was driven at a constant velocity $U(t) \equiv U_m=1.0$.

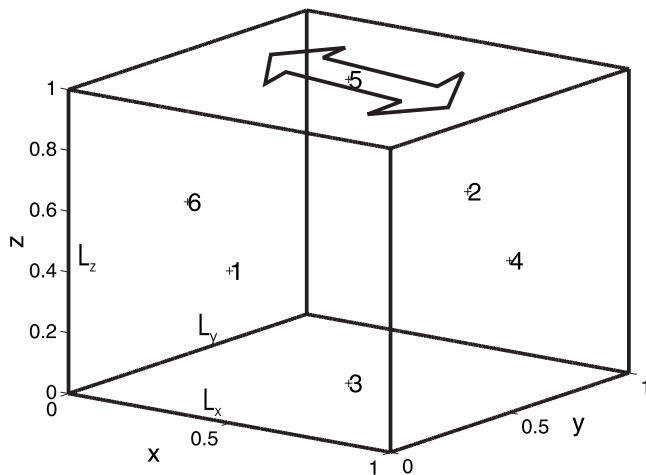


FIG. 8. Geometry of the cavity with a periodically driven lid.

A. Separation and attachment analyses

To analyze the time-averaged wall-shear field $\bar{\tau}$ on each wall shown in Fig. 9, we follow the steps described in the Sec. V F (details can be found in Surana *et al.*²³). Through these steps, we identify all separation and attachment points and curves and check their nondegeneracy. For brevity, we only show the final result of this analysis in Fig. 9. For separation patterns involving corner points, we have used the approach sketched in Sec. V D, described in detail by Surana *et al.*²³ We note that by symmetry of the flow, walls 1 and 2 admit identical wall-shear fields and corresponding separation patterns.

Note that wall 5 is not fixed and hence was analyzed in a frame comoving with it. The moving coordinate system leaves the flow domain, but nearby particle paths reveal that there is *no* separation or attachment on the moving wall despite the presence of zeros in the corresponding wall-shear field (see Fig. 9).

Figure 10 shows the local analytic predictions for the time-dependent separation (green) and attachment (blue) surfaces on walls 1, 3, 4, and 6, respectively. We have used the slope formulas (43) and (45) to obtain these approximate surfaces.

In Fig. 10, black curves represent the time-dependent wall-shear trajectories (see also Fig. 11). It is evident that, despite the large variations in the topology of the time-dependent wall-shear field, the separation and attachment occur at fixed locations. The particle paths shown in red and cyan validate this prediction.

VIII. CONCLUSIONS

In this paper, we have used nonlinear dynamical system techniques to give an exact treatment of fixed unsteady separation in 3D flows with a steady mean component. We have derived conditions under which time-dependent but boundary-fixed versions of the four basic separation patterns found in steady flows (see Surana *et al.*¹) arise. We have also derived exact first-order approximations to time-dependent separation curves and separation surfaces.

Our results cover separation near corners formed by no-slip boundaries and apply to curved moving boundaries after the transformations described by Surana *et al.*¹ For Navier–Stokes flows, the separation criteria and formulas obtained here can be expressed in terms of the wall shear and wall pressure; for details, we refer the reader to Surana *et al.*¹

We have illustrated our fixed unsteady separation criteria on time-dependent versions of analytic flow models derived by Surana *et al.*¹ and on a time-periodic lid-driven cavity

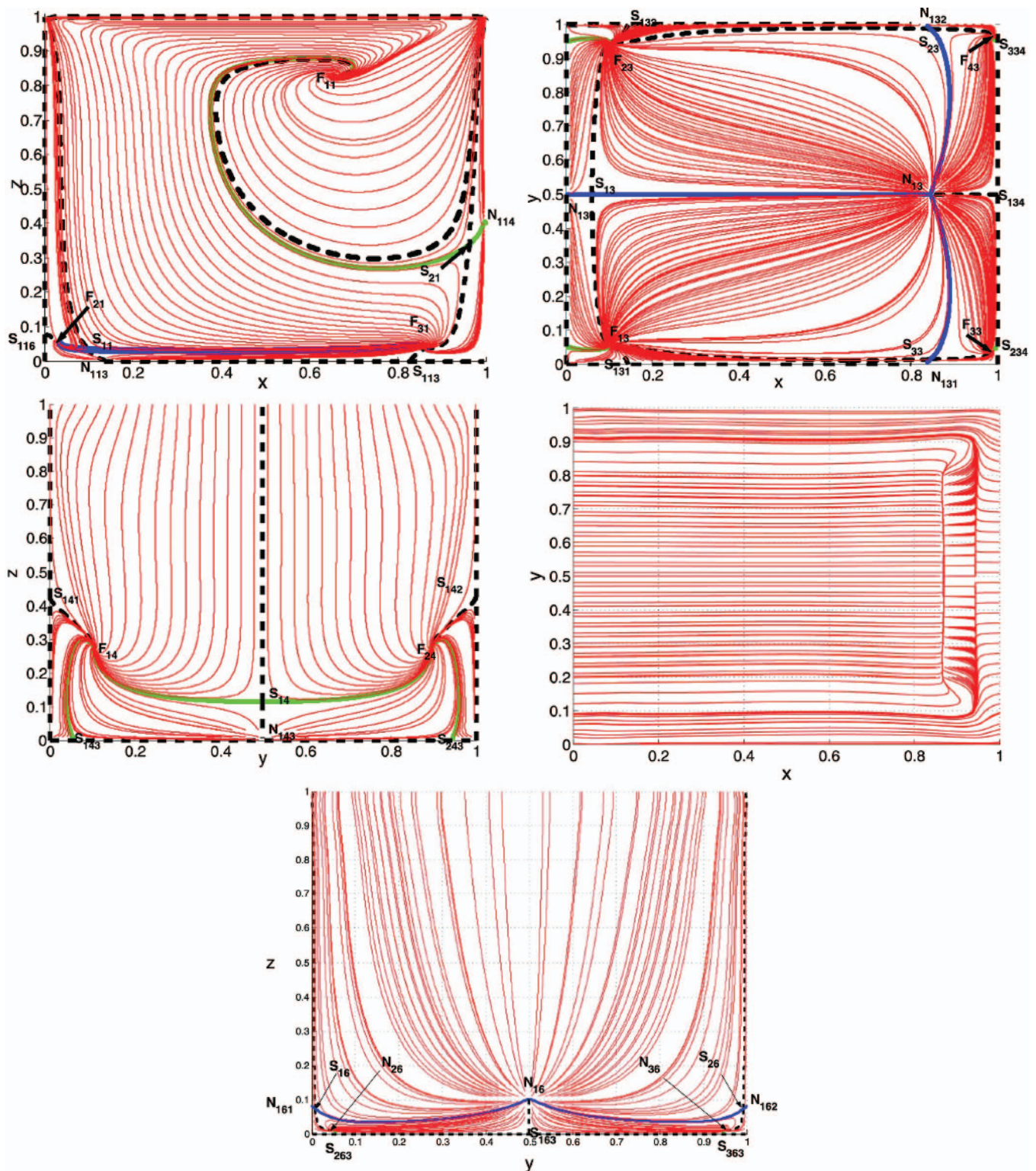


FIG. 9. (Color) Time averaged wall-shear fields on walls 1, 4, 5, and 6 for the time-periodic lid-driven cavity flow. We also indicate special averaged wall-shear lines (stable and unstable manifolds of the saddles) connecting averaged wall-shear zeros. Among these, the solid lines turn out to be actual separation lines (green) or attachment lines (blue).

flow. Separation over moving walls will be treated elsewhere.

Additional work is needed to characterize separation in turbulent flows with a time-varying mean component. An

example of such a flow is the velocity field around the wing of a maneuvering aircraft: The fast turbulent oscillations average out in the flow, but the slower maneuvering component of the motion is unsteady and its temporal average is typi-

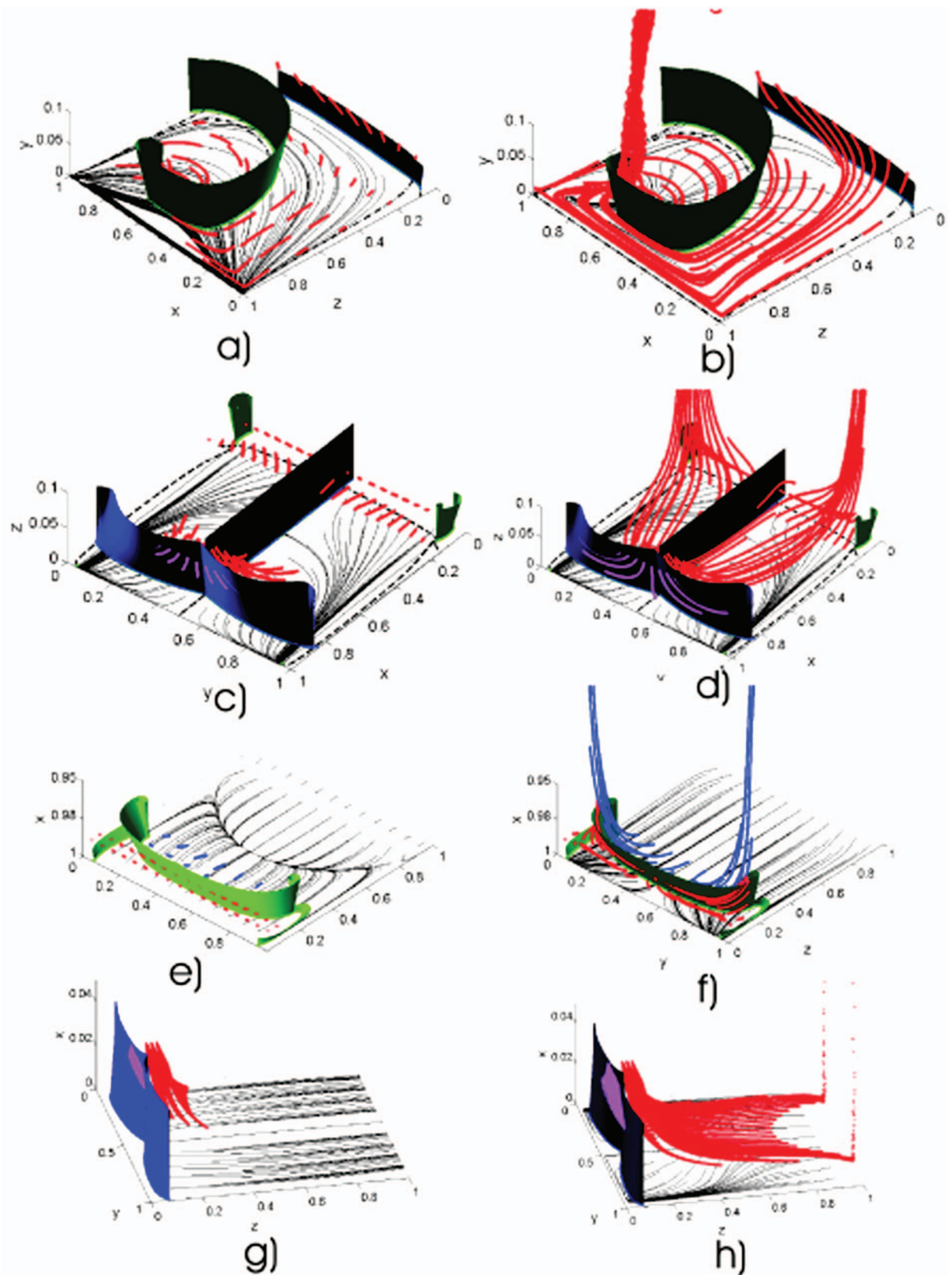


FIG. 10. (Color) Local approximation to the time-dependent separation and attachment surfaces which appear as green and blue, respectively, for different walls of the cavity. These predictions are validated by particle paths which have been colored red and cyan. The subplots (a) and (b) show wall 1, (c) and (d) show wall 3, (e) and (f) show wall 4, and (g) and (h) show wall 6.

cally nonzero. If the time scale of the mean component is sufficiently far from that of the oscillatory component, the separation location is no longer fixed: the flow displays moving separation. Moving separation turns out to occur along

finite-time unstable manifolds.⁸ Such finite-time manifolds can be located by extending the averaging techniques used in the present paper to flows with a slowly varying mean component.²²

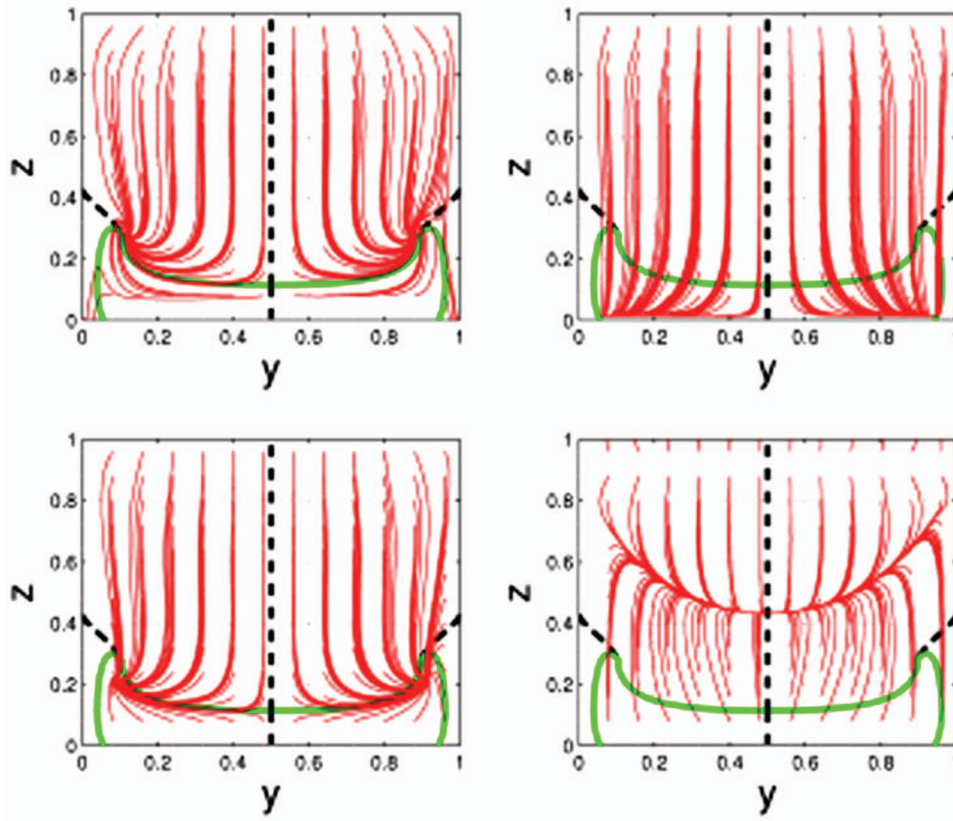


FIG. 11. (Color) Instantaneous wall-shear field (shown in red) on wall 4. We also indicate special averaged wall-shear lines (stable and unstable manifolds of the saddles) connecting averaged wall-shear zeros. Among these, the solid lines turn out to be actual separation lines (shown in green).

ACKNOWLEDGMENTS

This work was supported by AFOSR Grant No. FA9550-06-1-0101 and NSF Grant No. DMS-04-04845.

APPENDIX A: AVERAGED EQUATIONS

To derive the first-order averaged equation (19) from Eq. (17), we introduce the near-identity change of variables,

$$\boldsymbol{\eta} = \boldsymbol{\zeta} + \epsilon \mathbf{w}(\boldsymbol{\zeta}, t),$$

leading to

$$\begin{aligned} \dot{\boldsymbol{\eta}} &= \dot{\boldsymbol{\zeta}} + \epsilon \nabla_{\boldsymbol{\zeta}} \mathbf{w}(\boldsymbol{\zeta}, t) \dot{\boldsymbol{\zeta}} + \epsilon \partial_t \mathbf{w}(\boldsymbol{\zeta}, t) \\ &= \epsilon \mathbf{f}[\boldsymbol{\zeta} + \epsilon \mathbf{w}(\boldsymbol{\zeta}, t), t] + \epsilon^2 \mathbf{g}[\boldsymbol{\zeta} + \epsilon \mathbf{w}(\boldsymbol{\zeta}, t), t; \epsilon] \\ &= \epsilon \mathbf{f}(\boldsymbol{\zeta}, t) + \epsilon^2 [\nabla_{\boldsymbol{\zeta}} \mathbf{f}(\boldsymbol{\zeta}, t) \mathbf{w}(\boldsymbol{\zeta}, t) + \mathbf{g}(\boldsymbol{\zeta}, t; 0)] + \mathcal{O}(\epsilon^3). \end{aligned}$$

Rearranging gives

$$\begin{aligned} \dot{\boldsymbol{\zeta}} &= (\mathbf{I} + \epsilon \nabla_{\boldsymbol{\zeta}} \mathbf{w}(\boldsymbol{\zeta}, t))^{-1} \{ \epsilon [\mathbf{f}(\boldsymbol{\zeta}, t) - \partial_t \mathbf{w}(\boldsymbol{\zeta}, t)] \\ &\quad + \epsilon^2 [\nabla_{\boldsymbol{\zeta}} \mathbf{f}(\boldsymbol{\zeta}, t) \mathbf{w}(\boldsymbol{\zeta}, t) + \mathbf{g}(\boldsymbol{\zeta}, t; 0)] + \mathcal{O}(\epsilon^3) \}. \end{aligned}$$

For small ϵ , we have the expansion

$$[\mathbf{I} + \epsilon \nabla_{\boldsymbol{\zeta}} \mathbf{w}(\boldsymbol{\zeta}, t)]^{-1} = \mathbf{I} - \epsilon \nabla_{\boldsymbol{\zeta}} \mathbf{w}(\boldsymbol{\zeta}, t) + \mathcal{O}(\epsilon^2),$$

which gives

$$\begin{aligned} \dot{\boldsymbol{\zeta}} &= \epsilon [\mathbf{f}(\boldsymbol{\zeta}, t) - \partial_t \mathbf{w}(\boldsymbol{\zeta}, t)] + \epsilon^2 [\nabla_{\boldsymbol{\zeta}} \mathbf{f}(\boldsymbol{\zeta}, t) \mathbf{w}(\boldsymbol{\zeta}, t) + \mathbf{g}(\boldsymbol{\zeta}, t; 0) \\ &\quad + \nabla_{\boldsymbol{\zeta}} \mathbf{w}(\boldsymbol{\zeta}, t) \partial_t \mathbf{w}(\boldsymbol{\zeta}, t) - \nabla_{\boldsymbol{\zeta}} \mathbf{w}(\boldsymbol{\zeta}, t) \mathbf{f}(\boldsymbol{\zeta}, t)] + \mathcal{O}(\epsilon^3). \end{aligned}$$

Choosing

$$\mathbf{w}(\boldsymbol{\zeta}, t) = \int_{t_0}^t [\mathbf{f}(\boldsymbol{\zeta}, \tau) - \bar{\mathbf{f}}(\boldsymbol{\zeta})] d\tau,$$

$$\bar{\mathbf{f}}(\boldsymbol{\zeta}) = \lim_{T \rightarrow \infty} \frac{1}{T} \int_{t_0-T}^{t_0} \mathbf{f}(\boldsymbol{\zeta}, \tau) d\tau$$

for a given t_0 , we obtain the first-order averaged normal form,

$$\dot{\boldsymbol{\zeta}} = \epsilon \bar{\mathbf{f}}(\boldsymbol{\zeta}) + \epsilon^2 \mathbf{f}^1(\boldsymbol{\zeta}, t) + \mathcal{O}(\epsilon^3),$$

where

$$\begin{aligned} \mathbf{f}^1(\boldsymbol{\zeta}, t) &= \nabla_{\boldsymbol{\zeta}} \mathbf{f}(\boldsymbol{\zeta}, t) \mathbf{w}(\boldsymbol{\zeta}, t) - \nabla_{\boldsymbol{\zeta}} \mathbf{w}(\boldsymbol{\zeta}, t) \mathbf{f}(\boldsymbol{\zeta}, t) \\ &\quad + \nabla_{\boldsymbol{\zeta}} \mathbf{w}(\boldsymbol{\zeta}, t) \partial_t \mathbf{w}(\boldsymbol{\zeta}, t) + \mathbf{g}(\boldsymbol{\zeta}, t; 0) \\ &= \nabla_{\boldsymbol{\zeta}} \mathbf{f}(\boldsymbol{\zeta}, t) \mathbf{w}(\boldsymbol{\zeta}, t) + \mathbf{g}(\boldsymbol{\zeta}, t; 0) - \nabla_{\boldsymbol{\zeta}} \mathbf{w}(\boldsymbol{\zeta}, t) \bar{\mathbf{f}}(\boldsymbol{\zeta}). \end{aligned}$$

With $\boldsymbol{\zeta} = (\mathbf{q}, p)$ and

$$\bar{\boldsymbol{\tau}}(\mathbf{q}) = \lim_{T \rightarrow \infty} \frac{1}{T} \int_{t_0-T}^{t_0} \mathbf{A}_1(\mathbf{q}, 0, \tau) d\tau,$$

$$\phi(\mathbf{q}, t; t_0) = \int_{t_0}^t [\mathbf{A}_1(\mathbf{q}, 0, \tau) - \bar{\boldsymbol{\tau}}(\mathbf{q})] d\tau,$$

$$\bar{\mathbf{C}}(\mathbf{q}) = \lim_{T \rightarrow \infty} \frac{1}{T} \int_{t_0-T}^{t_0} \mathbf{C}_1(\mathbf{q}, 0, \tau) d\tau,$$

$$\psi(\mathbf{q}, t; t_0) = \int_{t_0}^t [C_1(\mathbf{q}, 0, t) - \bar{C}(\mathbf{q})] d\tau,$$

we can express $\bar{\mathbf{f}}$ as

$$\bar{\mathbf{f}}(\boldsymbol{\xi}) = \begin{pmatrix} p\bar{\boldsymbol{\tau}}(\mathbf{q}) \\ p^2\bar{C}(\mathbf{q}) \end{pmatrix}.$$

Similarly we can express \mathbf{f}^1 as

$$\mathbf{f}^1(\boldsymbol{\xi}, t) = \begin{pmatrix} p^2\mathbf{F}(\mathbf{q}, t) \\ p^3G(\mathbf{q}, t) \end{pmatrix},$$

where

$$\mathbf{F}(\mathbf{q}, t) = [\nabla_{\mathbf{x}}\mathbf{A}_1(\mathbf{q}, 0, t) - \bar{C}\mathbf{1}] \phi - \nabla_{\mathbf{x}}\phi\bar{\boldsymbol{\tau}} + \partial_z\mathbf{A}_1(\mathbf{q}, 0, t) + \mathbf{A}_1(\mathbf{q}, 0, t)\psi,$$

$$G(\mathbf{q}, t) = 2[C_1(\mathbf{q}, 0, t) - \bar{C}] - \nabla_{\mathbf{x}}\psi \cdot \bar{\boldsymbol{\tau}}\psi + \partial_z C_1(\mathbf{q}, 0, t) + \nabla_{\mathbf{x}}C_1(\mathbf{q}, 0, t) \cdot \phi,$$

with \cdot denoting the standard inner product.

The second-order averaged form is obtained in a similar manner. Specifically, we eliminate the time dependence in \mathbf{f}^1 by introducing the change of variables,

$$\boldsymbol{\zeta} = \boldsymbol{\xi} + \epsilon^2\mathbf{h}(\boldsymbol{\xi}, t),$$

$$\mathbf{h}(\boldsymbol{\xi}, t) = \int_{t_0}^t [\mathbf{f}^1(\boldsymbol{\xi}, t) - \bar{\mathbf{f}}^1(\boldsymbol{\xi})] d\tau.$$

We follow the same procedure as above to obtain

$$\dot{\boldsymbol{\zeta}} = \epsilon\bar{\mathbf{f}}(\boldsymbol{\xi}) + \epsilon^2\bar{\mathbf{f}}^1(\boldsymbol{\xi}) + \mathcal{O}(\epsilon^3), \quad (\text{A1})$$

where

$$\bar{\mathbf{f}}^1(\boldsymbol{\xi}) = \lim_{T \rightarrow \infty} \frac{1}{T} \int_{t_0-T}^{t_0} \mathbf{f}^1(\boldsymbol{\xi}, \tau) d\tau = \begin{pmatrix} s^2\bar{F}(\mathbf{r}) \\ s^3\bar{G}(\mathbf{r}) \end{pmatrix},$$

with $\boldsymbol{\xi} = (\mathbf{r}, s)$ and

$$\bar{F} = \lim_{T \rightarrow \infty} \frac{1}{T} \int_{t_0-T}^{t_0} \mathbf{F}(\mathbf{r}, \tau) d\tau,$$

$$\bar{G} = \lim_{T \rightarrow \infty} \frac{1}{T} \int_{t_0-T}^{t_0} G(\mathbf{r}, \tau) d\tau.$$

In component form, we can rewrite Eq. (A1) as

$$\dot{\mathbf{r}} = \epsilon s[\bar{\boldsymbol{\tau}}(\mathbf{r}) + s\epsilon\bar{\mathbf{F}}(\mathbf{r})] + \mathcal{O}(\epsilon^3), \quad (\text{A2})$$

$$\dot{s} = \epsilon s^2[\bar{C}(\mathbf{r}) + s\epsilon\bar{G}(\mathbf{r})] + \mathcal{O}(\epsilon^3).$$

APPENDIX B: PERSISTENCE OF SEPARATION PATTERNS IN THE FULL FLOW

In this appendix, we prove Theorem 1 of Sec. V B and Theorem 2 of Sec. V C. The proof relies on topological invariant manifold techniques that we apply on a case-by-case basis.

1. Persistence of separation curves: Node and spiral

For system (27), the point $(\mathbf{p}, 0)$ is a separation point if and only if¹

$$\bar{\boldsymbol{\tau}}(\mathbf{p}) = 0, \quad \nabla_{\mathbf{x}} \cdot \bar{\boldsymbol{\tau}}(\mathbf{p}) < 0, \quad (\text{B1})$$

$$\det \nabla_{\mathbf{x}} \bar{\boldsymbol{\tau}}(\mathbf{p}) > 0, \quad \bar{C}(\mathbf{p}) > 0.$$

Here we show that under the same conditions, the unstable manifold emanating from \mathbf{p} persists in the full system (19). This result is not obvious because the no-slip boundary conditions make the unstable manifold degenerate (nonhyperbolic), and hence its survival under small perturbations is not guaranteed by classic dynamical system results.

Recall that the first-order averaged normal form (19) in the component form $\boldsymbol{\zeta} = (\mathbf{q}, p)$ is given by

$$\dot{\mathbf{q}} = \epsilon p \bar{\boldsymbol{\tau}}(\mathbf{q}) + \epsilon^2 p^2 \mathbf{n}_1(\mathbf{q}, p, \epsilon, t), \quad (\text{B2})$$

$$\dot{p} = \epsilon p^2 \bar{C}(\mathbf{q}) + \epsilon^2 p^3 n_2(\mathbf{q}, p, \epsilon, t),$$

where the $\mathcal{O}(\epsilon^2)$ terms are bounded by our assumptions. By making the change of coordinates $\mathbf{q} \rightarrow \mathbf{q} - \mathbf{x}_0$, where \mathbf{x}_0 is any point on the boundary, we transform the first-order averaged equations (B2) to the form

$$\begin{aligned} \dot{\mathbf{q}} = & \epsilon p \bar{\boldsymbol{\tau}}(\mathbf{x}_0) + \epsilon p \nabla_{\mathbf{x}} \bar{\boldsymbol{\tau}}(\mathbf{x}_0) \cdot \mathbf{q} + \epsilon p [\mathbf{m}_1(\mathbf{q}, p, \epsilon, t) q_1^2 \\ & + \mathbf{m}_2(\mathbf{q}, p, \epsilon, t) q_1 q_2 + \mathbf{m}_3(\mathbf{q}, p, \epsilon, t) q_2^2] \\ & + \epsilon^2 p^2 \mathbf{m}_4(\mathbf{q}, p, \epsilon, t), \end{aligned} \quad (\text{B3})$$

$$\dot{p} = \epsilon p^2 \bar{C}(\mathbf{x}_0) + \epsilon^2 p^3 m_5(\mathbf{q}, p, \epsilon, t) + \epsilon p^2 \mathbf{q} \cdot \mathbf{m}_6(\mathbf{q}, p, \epsilon, t),$$

where \mathbf{m}_i are appropriate smooth functions that are uniformly bounded in their arguments, notably in t .

Choosing $\mathbf{x}_0 = \mathbf{p}$ in Eq. (B3), we obtain

$$\dot{\mathbf{q}} = \epsilon p \nabla_{\mathbf{x}} \bar{\boldsymbol{\tau}}(\mathbf{p}) \cdot \mathbf{q} + \epsilon p [\mathbf{m}_1 q_1^2 + \mathbf{m}_2 q_1 q_2 + \mathbf{m}_3 q_2^2] + \epsilon^2 p^2 \mathbf{m}_4, \quad (\text{B4})$$

$$\dot{p} = \epsilon p^2 \bar{C}(\mathbf{p}) + \epsilon^2 p^3 m_5 + \epsilon p^2 \mathbf{q} \cdot \mathbf{m}_6$$

as transformed equations of motion for fluid particles near \mathbf{p} .

Consider the solid cone

$$Q = \{(\mathbf{q}, p) \mid \|\mathbf{q}\| \leq \alpha p, \quad 0 \leq p \leq \beta\},$$

where α and β are positive constants to be selected below (Fig. 12). The lateral surface L of this cone is

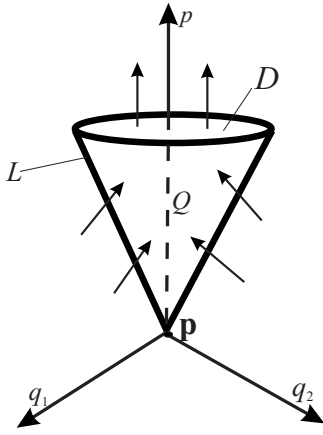
$$L = \{(\mathbf{q}, p) \in Q \mid \|\mathbf{q}\| = \alpha p\}, \quad (\text{B5})$$

which can be parametrized by $q_1 = \alpha p \cos(\theta)$, $q_2 = \alpha p \sin(\theta)$, where $\theta \in [0, 2\pi)$ and $\alpha = \tan(\psi)$ with ψ denoting the half-angle of the cone. The outward unit normal \mathbf{n} to Q can be written as

$$\mathbf{n} = \frac{1}{\sqrt{1 + \alpha^2}} \begin{pmatrix} \cos(\theta) \\ \sin(\theta) \\ -\alpha \end{pmatrix}. \quad (\text{B6})$$

Finally, the top disk D of the cone can be described as

$$D = \{(\mathbf{q}, p) \in Q \mid p = \beta\}. \quad (\text{B7})$$

FIG. 12. Geometry of the set Q .

Restricted to the disk D , the particle equations of motion become

$$\begin{aligned} \dot{p}|_{p=\beta} &= \epsilon\beta^2[\bar{C}(\mathbf{p}) + \epsilon\beta m_5 + \mathbf{q} \cdot \mathbf{m}_6] \\ &\geq \epsilon\beta^2[\bar{C}(\mathbf{p}) - \epsilon p|m_5| - |\mathbf{q}| \cdot |m_6|] \geq \epsilon\beta^2 \frac{\bar{C}(\mathbf{p})}{2} > 0, \end{aligned}$$

provided that we choose ϵ and β appropriately small. Therefore, solutions intersecting the D leave Q immediately if $\bar{C}(\mathbf{p}) > 0$ and ϵ and β are small enough.

Now consider the L boundary of the cone Q , for which $\mathbf{q} = \alpha p \mathbf{e}$, where $\mathbf{e} = (\cos \theta, \sin \theta)^T$, and hence

$$\begin{aligned} \dot{\mathbf{q}}|_{\mathbf{q}=\alpha p \mathbf{e}} &= \epsilon p^2 \{ \alpha \nabla_{\mathbf{x}} \bar{\tau}(\mathbf{p}) \mathbf{e} + p \alpha^2 [\mathbf{m}_1 \cos^2(\theta) \\ &\quad + \mathbf{m}_2 \cos(\theta) \sin(\theta) + \mathbf{m}_3 \sin^2(\theta)] + \epsilon \mathbf{m}_4 \}, \end{aligned}$$

$$\dot{p}|_{\mathbf{q}=\alpha p \mathbf{e}} = \epsilon p^2 [\bar{C}(\mathbf{p}) + \epsilon p m_5 + \alpha p \mathbf{e} \cdot \mathbf{m}_6].$$

The flow enters the cone on this surface, provided

$$\mathbf{n} \cdot (\dot{\mathbf{q}}, \dot{p}) < 0 \quad (\text{B8})$$

everywhere on the surface. This is the case if

$$\alpha \dot{p}|_{\alpha p \mathbf{e}} > \dot{\mathbf{q}}|_{\alpha p \mathbf{e}} \cdot \mathbf{e} \quad \text{for any } \theta \text{ and } 0 < p \leq \beta,$$

or equivalently,

$$\begin{aligned} \alpha [\bar{C}(\mathbf{p}) - \mathbf{e} \cdot \nabla_{\mathbf{x}} \bar{\tau}(\mathbf{p}) \mathbf{e}] + \epsilon \alpha p m_5 - \epsilon \mathbf{m}_4 \cdot \mathbf{e} \\ - p \alpha^2 [\mathbf{m}_1 \cdot \mathbf{e} \cos^2(\theta) + \mathbf{m}_3 \cdot \mathbf{e} \sin^2(\theta)] \\ + p \alpha^2 [\mathbf{e} \cdot \mathbf{m}_6 - \mathbf{m}_2 \cdot \mathbf{e} \cos(\theta) \sin(\theta)] > 0 \end{aligned}$$

for any θ and for all $0 < p \leq \beta$. By choosing $\alpha = 1$, and setting ϵ and β sufficiently small, we can make the above inequality satisfied provided that

$$\bar{C}(\mathbf{p}) - \lambda_{\max}[\nabla_{\mathbf{x}} \bar{\tau}(\mathbf{p})] > 0, \quad (\text{B9})$$

where $\lambda_{\max}[\nabla_{\mathbf{x}} \bar{\tau}(\mathbf{p})]$ is the maximum singular value of the Jacobian of the wall-shear field evaluated at the separation point \mathbf{p} . The second and third inequalities in Eq. (B1) imply $\lambda_{\max}[\nabla_{\mathbf{x}} \bar{\tau}(\mathbf{p})] < 0$. This, along with the last inequality in Eq. (B1), implies that condition (B9) is always satisfied. From

this we conclude that solutions intersecting the L boundary of the cone Q enter Q immediately.

a. Solutions staying in Q in backward time converge to \mathbf{p}

We next examine the asymptotic behavior of solutions staying in the cone for all backward times, from which we shall later conclude the existence of an unstable manifold for \mathbf{p} .

Consider an initial position $(\mathbf{q}_0, p_0) \in Q$ at t_0 and denote the trajectory starting from this initial position by $(\mathbf{q}(t), p(t))$. Integration of

$$\dot{p}(t) = \epsilon p(t)^2 [\bar{C}(\mathbf{p}) + \epsilon p m_5 + \mathbf{q} \cdot \mathbf{m}_6]_{(\mathbf{q}(t), p(t))} \quad (\text{B10})$$

gives

$$p(t) = \frac{p_0}{1 + \epsilon p_0 \int_{t_0}^t [\bar{C}(\mathbf{p}) + \epsilon p(\tau) m_5 + \mathbf{q} \cdot \mathbf{m}_6] d\tau}. \quad (\text{B11})$$

If the trajectory starting from (\mathbf{q}_0, p_0) stays in Q for all backward times, Eq. (B11) holds for all $t \leq t_0$. Choosing ϵ and β appropriately small then leads to the estimate

$$\begin{aligned} p(t) &\leq \frac{p_0}{1 + \epsilon p_0 \int_{t_0}^t [\bar{C}(\mathbf{p}) - \epsilon p|m_5| - |\mathbf{q}| \cdot |m_6|] d\tau} \\ &\leq \frac{p_0}{1 + \frac{\epsilon p_0}{2} \bar{C}(\mathbf{p})(t_0 - t)}. \end{aligned}$$

This allows us to conclude that

$$\lim_{t \rightarrow -\infty} p(t) = 0.$$

In other words, trajectories that never leave Q in backward time will necessarily converge to the $p=0$ boundary of the cone Q . By the definition of Q , however, this convergence in the p direction implies

$$\lim_{t \rightarrow -\infty} \mathbf{q}(t) = 0.$$

b. All solutions leave Q in forward time

For any $p_0 > 0$, consider an initial position $(\mathbf{q}_0, p_0) \in Q$ at time t_0 ; denote the trajectory starting from this initial position by $(\mathbf{q}(t), p(t))$. In forward time, the trajectory cannot leave the cone through L . We show that the p coordinate grows and reaches β in a uniform finite time for any given $p_0 > 0$. Hence, the trajectory must exit the cone through D .

By our discussion in Appendix B 1 a, along the trajectory starting from (\mathbf{q}_0, p_0) , we have

$$\begin{aligned} p(t) &\geq \frac{p_0}{1 - \epsilon p_0 \int_{t_0}^t [\bar{C}(\mathbf{p}) - \epsilon p|m_5| - |\mathbf{q}| \cdot |m_6|] d\tau} \\ &\geq \frac{p_0}{1 - \epsilon p_0 \frac{\bar{C}(\mathbf{p})}{2} (t - t_0)}, \end{aligned}$$

which holds for $t > t_0$ while the trajectory stays in Q in for-

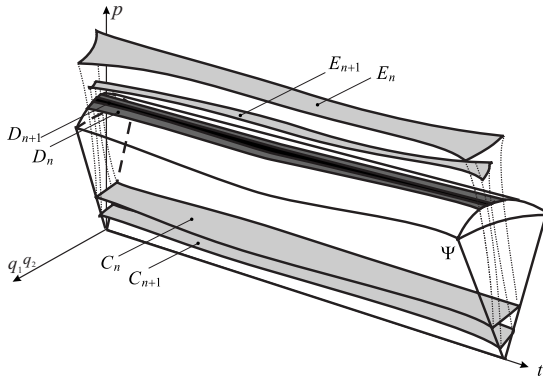


FIG. 13. The cylinders C_n and D_n are shown schematically in the extended phase space.

ward time. Then, if $p_0 \neq 0$, then the relation $p(t) \leq \beta$ is violated at times

$$t > t_0 + \frac{2}{\epsilon \bar{C}(\mathbf{p})} \left[\frac{1}{p_0} - \frac{1}{\beta} \right]. \quad (\text{B12})$$

Thus, the trajectory has to leave the cone through D .

c. There exist solutions that stay in Q for all backward times

To prove that there are solutions that stay in Q for all backward times, we follow the argument developed by Haller.²⁷ In the extended phase space of the (\mathbf{q}, p, t) variables, let

$$\Psi = Q \times \mathbb{R}, \quad \mathcal{L} = L \times \mathbb{R}, \quad \mathcal{D} = D \times \mathbb{R}. \quad (\text{B13})$$

Consider an infinite sequence of closed curves $\{C_n\}_{n=1}^{\infty}$ with $C_n \in L$ such that each C_n encircles the p axis and $\lim_{n \rightarrow \infty} C_n = 0$. In the extended phase space, each family of circles C_n appears as an infinite cylinder,

$$C_n = \{(\mathbf{q}, p, t) | \mathbf{q} \in C_n, t \in \mathbb{R}\}, \quad (\text{B14})$$

as shown in Fig. 13.

By our discussion in Appendix B 1 b above, we conclude that there exists a finite time $T_n > 0$ (B12), such that at time $t + T_n$, all solutions (\mathbf{q}, p, t) starting from the cylinder C_n are outside Q . At time T_n , the image of the cylinder C_n under the flow map is E_n , as shown in the Fig. 13. All trajectories evolving from C_n in forward time intersect the boundary of \mathcal{D} forming another cylinder D_n , as shown in Fig. 13. Similarly, the cylinder C_{n+1} gives rise to a cylinder $D_{n+1} \subset D_n$ on the boundary of \mathcal{D} . By construction, any solutions starting from $D_n \setminus D_{n+1}$ exit \mathcal{C} somewhere between the circles C_n and C_{n+1} in backward time. The infinite sequence of cylinders, $D_1 \supset D_2 \supset \dots$, is a nested sequence of nonempty closed set, and hence

$$D^\infty = \bigcap_{n \geq 1} D_n \quad (\text{B15})$$

is a nonempty curve by Cantor's theorem. Observe that a point $(\mathbf{q}^*, p^*, t^*) \in D^\infty$ will never exit Q in backward time because there is no index N for which $(\mathbf{q}^*, p^*, t^*) \in D_N \setminus D_{N+1}$. For any time t^* , therefore, we have found an

initial condition (\mathbf{q}^*, p^*) such that the corresponding solution $[\mathbf{q}^*(t), p^*(t)]$ stays in Q for all $t \leq t^*$.

d. Existence of unstable manifold

From Appendix B 1 a above, we obtain that $[\mathbf{q}^*(t), p^*(t)]$ converges to the origin (the tip of the cone Q) in backward time. Thus, we have shown that there is a nonempty set of initial fluid particle positions W^∞ that stay in Q for all backward times. By definition, W^∞ is an invariant set that is necessarily smooth in t because it is composed of fluid trajectories that are smooth in t . We, therefore, conclude that all trajectories in W^∞ converge to $p = \mathbf{q} = 0$ in backward time, thus W^∞ is an unstable manifold for $(\mathbf{p}, 0)$.

By reversing the time direction in all the above arguments, we conclude the persistence of an attachment profile (stable manifold) under the conditions

$$\bar{\boldsymbol{\tau}}(\mathbf{p}) = 0, \quad \nabla_{\mathbf{x}} \cdot \bar{\boldsymbol{\tau}}(\mathbf{p}) > 0,$$

$$\det \nabla_{\mathbf{x}} \bar{\boldsymbol{\tau}}(\mathbf{p}) > 0, \quad \bar{C}(\mathbf{p}) < 0,$$

and hence Eq. (33) follows.

2. Persistence of separation surfaces: Saddle connections and limit cycles

Consider a bounded wall-shear line γ of the time averaged wall-shear field $\bar{\boldsymbol{\tau}}$. As shown by Surana *et al.*,¹ γ is the separation line for the averaged steady velocity fields if the following is satisfied:

- (1) γ originates from a saddle \mathbf{p} with $\bar{C}(\mathbf{p}) > 0$ and ends at a stable spiral \mathbf{q} with $\bar{C}(\mathbf{q}) > 0$.
- (2) γ originates from a saddle \mathbf{p} with $\bar{C}(\mathbf{p}) > 0$ and ends at a stable node \mathbf{q} with $\bar{C}(\mathbf{q}) > 0$. Also, γ is tangent to the direction of weaker attraction at \mathbf{q} .
- (3) γ originates from a saddle \mathbf{p} with $\bar{C}(\mathbf{p}) > 0$ and spirals onto a stable limit cycle Γ with $\int_{\Gamma} \bar{C} ds > 0$.
- (4) γ is a stable limit cycle with $\int_{\gamma} \bar{C} ds > 0$.

Similarly, γ is an attachment line if the following is satisfied:

- (1) γ originates at a unstable spiral \mathbf{p} with $\bar{C}(\mathbf{p}) < 0$ and ends at a saddle \mathbf{q} with $\bar{C}(\mathbf{q}) < 0$.
- (2) γ originates at a unstable node \mathbf{p} with $\bar{C}(\mathbf{p}) < 0$ and ends at a saddle \mathbf{q} with $\bar{C}(\mathbf{q}) < 0$. Also, γ is tangent to the direction of weaker repulsion at \mathbf{p} .
- (3) γ spirals off from an unstable limit cycle Γ with $\int_{\Gamma} \bar{C} ds < 0$ and ends at a saddle \mathbf{q} with $\bar{C}(\mathbf{q}) < 0$.
- (4) γ is a unstable limit cycle with $\int_{\gamma} \bar{C} ds < 0$.

Below we show that under the stronger pointwise assumptions,

$$\bar{S}_{\perp}(\mathbf{x}) - \bar{C}(\mathbf{x}) < 0, \quad \bar{C}(\mathbf{x}) > 0, \quad (\text{B16})$$

on all points \mathbf{x} in γ , the four basic separation patterns (1)–(4) inferred based on the steady limit (27) persist in the full flow (19). Under the assumptions

$$\bar{S}_\perp(\mathbf{x}) - \bar{C}(\mathbf{x}) > 0, \quad \bar{C}(\mathbf{x}) < 0, \quad \forall \mathbf{x} \in \gamma, \quad (\text{B17})$$

a similar conclusion holds for the four basic attachment patterns (1)–(4), leading to the results discussed in Sec. V C.

The proof of above results relies on *Wasewsky principle*, which we recall briefly for convenience following the formulation given by Conley.²⁸

a. The Wasewsky principle

Suppose Ω is an open set in \mathbb{R}^n , $f: \Omega \rightarrow \mathbb{R}^n$ is a continuous map and let

$$\phi: \mathbf{x}_0 \mapsto \mathbf{x}(t; \mathbf{x}_0)$$

[with $\mathbf{x}(0; \mathbf{x}_0) = \mathbf{x}_0$] be the flow map of the ordinary differential equation,

$$\dot{\mathbf{x}} = f(\mathbf{x}). \quad (\text{B18})$$

We shall denote the *closure* of W in Ω by \bar{W} and define

$$\Phi(\mathbf{x}, \mathcal{I}) = \{\phi(\mathbf{x}, t) | t \in \mathcal{I}\},$$

where $\mathcal{I} \subset \mathbb{R}$.

Let $W \subset \Omega$ be any set and consider the sets

$$W^{\text{ev}} = \{\mathbf{x} \in W | \exists t > 0, s. \text{ t. } \phi(\mathbf{x}, t) \notin W\},$$

$$W^{\text{im}} = \{\mathbf{x} \in W | \Phi(\mathbf{x}, [0, t]) \subsetneq W, \forall t > 0\}.$$

W is called a forward time Wasewsky set if the following conditions are satisfied:

- (1) If $\mathbf{x} \in W$ and $\Phi(\mathbf{x}, [0, t]) \subset \bar{W}$, then $\Phi(\mathbf{x}, [0, t]) \subset W$.
- (2) W^{im} is closed relative to W^{ev} .

The Wasewsky principle states the following: If W is a Wasewsky set then W^{im} is a strong deformation retract of W^{ev} and W^{ev} is open relative to W .

An important quantity introduced in the proof of the above result is the time map $\tau: W^{\text{ev}} \rightarrow \mathbf{R}$, defined as

$$\tau(\mathbf{x}) = \sup\{t \geq 0 | \Phi([0, t], \mathbf{x}) \subset W\}.$$

By the definition of W^{ev} , $\tau(\mathbf{x})$ is finite, and by continuity of the flow, we have $\Phi(\mathbf{x}, [0, \tau(\mathbf{x})]) \subset \bar{W}$. Thus, by property (1) above, we have $\phi(\mathbf{x}, \tau(\mathbf{x})) \in W$. Now from the definition of τ , $\phi(\tau(\mathbf{x}), \mathbf{x}) \in W^{\text{im}}$ and $\tau(\mathbf{x}) = 0$ for $\mathbf{x} \in W^{\text{im}}$. This leads to the following corollary.

Corollary: The Wasewsky map $\Gamma: W^{\text{ev}} \rightarrow W^{\text{im}}$ defined as

$$\Gamma(\mathbf{x}) = \phi[\mathbf{x}, \tau(\mathbf{x})] \quad (\text{B19})$$

is continuous. It is this last corollary of the Wasewsky principle that we shall use below in our arguments.

b. Transformed equations of motion

We begin our persistence proof by introducing new coordinates along a separation line γ identified from the first-order averaged normal form. At any point $\mathbf{x} = \mathbf{x}(s, \mathbf{x}_0) \in \gamma$, the unit tangent $\mathbf{t}(s)$ and the unit normal $\mathbf{n}(s)$ to γ are given by

$$\mathbf{t}(s) = \frac{\bar{\boldsymbol{\tau}}}{|\bar{\boldsymbol{\tau}}|} \Big|_{\mathbf{x}(s, \mathbf{x}_0)}, \quad \mathbf{n}(s) = \frac{\bar{\boldsymbol{\omega}}}{|\bar{\boldsymbol{\omega}}|} \Big|_{\mathbf{x}(s, \mathbf{x}_0)}, \quad (\text{B20})$$

respectively, where $\mathbf{x}(s, \mathbf{x}_0)$ is the wall-shear trajectory with $\mathbf{x}(0, \mathbf{x}_0) = \mathbf{x}_0$. Let $[x(s_p), y(s_p)] \in \mathbf{x}(s, \mathbf{x}_0)$. We change coordinates through

$$\begin{pmatrix} \mathbf{q} \\ p \end{pmatrix} = T_p \begin{pmatrix} \eta_1 \\ \eta_2 \\ \eta_3 \end{pmatrix}, \quad (\text{B21})$$

with

$$T_p = \begin{pmatrix} \mathbf{t}(s_p) & \mathbf{n}(s_p) & 0 \\ 0 & 0 & 1 \end{pmatrix}, \quad (\text{B22})$$

to obtain from Eq. (B3) the new equations of particle motion

$$\begin{aligned} \dot{\eta}_1 &= \epsilon \eta_3 |\bar{\boldsymbol{\tau}}[x(s_p), y(s_p)]| + \epsilon \eta_3 \eta_1 \bar{S}_{\parallel} \{[x(s_p), y(s_p)]\} \\ &\quad + \epsilon \eta_3 \eta_2 \bar{S}_{\perp} \{[x(s_p), y(s_p)]\} \\ &\quad + \epsilon \eta_3 [h_1(\boldsymbol{\eta}, \epsilon, t) \eta_1^2 + h_2(\boldsymbol{\eta}, \epsilon, t) \eta_1 \eta_2 + h_3(\boldsymbol{\eta}, \epsilon, t) \eta_2^2] \\ &\quad + \epsilon^2 \eta_3^2 h_4(\boldsymbol{\eta}, \epsilon, t), \end{aligned} \quad (\text{B23})$$

$$\begin{aligned} \dot{\eta}_2 &= \epsilon \eta_3 \eta_1 \bar{S}_{\perp} \{[x(s_p), y(s_p)]\} + \epsilon \eta_3 \eta_2 \bar{S}_{\parallel} \{[x(s_p), y(s_p)]\} \\ &\quad + \epsilon \eta_3 [h_5(\boldsymbol{\eta}, \epsilon, t) \eta_1^2 + h_6(\boldsymbol{\eta}, \epsilon, t) \eta_1 \eta_2 + h_7(\boldsymbol{\eta}, \epsilon, t) \eta_2^2] \\ &\quad + \epsilon^2 \eta_3^2 h_8(\boldsymbol{\eta}, \epsilon, t), \end{aligned} \quad (\text{B24})$$

$$\begin{aligned} \dot{\eta}_3 &= \epsilon \eta_3^2 \{\bar{C}[x(s_p), y(s_p)] + \epsilon \eta_3 h_9(\boldsymbol{\eta}, \epsilon, t) + \eta_1 h_{10}(\boldsymbol{\eta}, \epsilon, t) \\ &\quad + \eta_2 h_{11}(\boldsymbol{\eta}, \epsilon, t)\}. \end{aligned} \quad (\text{B25})$$

In the above equations, $h_i(\boldsymbol{\eta}, \epsilon, t)$ are appropriate smooth and bounded functions in all the arguments and

$$\bar{S}_{\parallel}[x(s_p), y(s_p)] = \langle \mathbf{t}, \nabla_{\mathbf{x}} \bar{\boldsymbol{\tau}} \rangle \Big|_{\mathbf{x}=[x(s_p), y(s_p)]},$$

$$\bar{S}_{\perp}[x(s_p), y(s_p)] = \langle \mathbf{n}, \nabla_{\mathbf{x}} \bar{\boldsymbol{\tau}} \rangle \Big|_{\mathbf{x}=[x(s_p), y(s_p)]},$$

$$\bar{S}_{\parallel}[x(s_p), y(s_p)] = \langle \mathbf{t}, \nabla_{\mathbf{x}} \bar{\boldsymbol{\omega}} \rangle \Big|_{\mathbf{x}=[x(s_p), y(s_p)]},$$

$$\bar{S}_{\perp}[x(s_p), y(s_p)] = \langle \mathbf{n}, \nabla_{\mathbf{x}} \bar{\boldsymbol{\omega}} \rangle \Big|_{\mathbf{x}=[x(s_p), y(s_p)]}.$$

c. Persistence of separation surface near a saddle

Consider a nondegenerate saddle $(\mathbf{p}, 0)$ of the time-averaged wall-shear field; it will satisfy

$$\bar{\boldsymbol{\tau}}(\mathbf{p}) = 0, \quad \det \nabla_{\mathbf{x}} \bar{\boldsymbol{\tau}}(\mathbf{p}) < 0, \quad \bar{C}(\mathbf{p}) > 0.$$

Let $\mathbf{x}_1(s), s \in \mathcal{I}_1 = [-s_-, 0]$ and $\mathbf{x}_2(s), s \in \mathcal{I}_2 = [0, s_+]$ be the two branches of the unstable manifold in the vicinity of \mathbf{p} such that $\mathbf{x}_1(0) = \mathbf{x}_2(0) = \mathbf{p}$, where $s_- > 0$ and $s_+ > 0$ are to be chosen later. Define

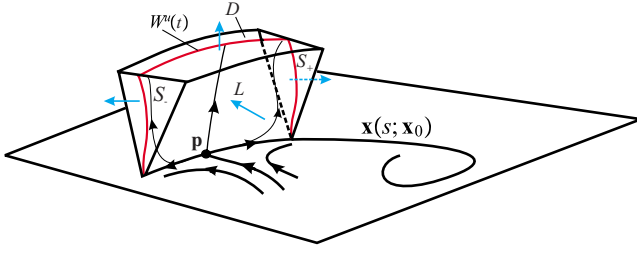


FIG. 14. (Color online) Wasewsky set near a saddle.

$$\gamma_v = \mathbf{x}_1(s) \cup \mathbf{x}_2(s), \quad s \in \mathcal{I} = \mathcal{I}_1 \cup \mathcal{I}_2,$$

which is just a subset of the separation line in the vicinity of \mathbf{p} . We construct a cone section along γ parametrized by $s_p \in \mathcal{I}$ as follows:

$$Q_{s_p} = \{(\eta_1, \eta_2, \eta_3) \mid \eta_1 = 0, |\eta_2| \leq \eta_3, 0 \leq \eta_3 \leq \beta(s_p)\},$$

where $\beta(s)$ is a positive continuous function to be selected below (see Fig. 14). The lateral side L_{s_p} of Q_{s_p} is given by

$$L_{s_p} = \{(\eta_1, \eta_2, \eta_3) \in Q_{s_p} \mid |\eta_2| = \eta_3\}.$$

The top of the cone will be denoted by D_{s_p} ,

$$D_{s_p} = \{(\eta_1, \eta_2, \eta_3) \in Q_{s_p} \mid \eta_3 = \beta(s_p)\}.$$

Along the boundary D_{s_p} of the cone, the inequality

$$\begin{aligned} \dot{\eta}_3|_{\{\eta \in D_{s_p}\}} &= \epsilon \beta^2(s_p) \{ \bar{C}[x(s_p), y(s_p)] + \epsilon \beta(s_p) h_9 + \eta_2 h_{11} \} \\ &\geq \epsilon \beta^2(s_p) \frac{\bar{C}[x(s_p), y(s_p)]}{2} > 0 \end{aligned} \quad (\text{B26})$$

holds, provided that we choose ϵ and $\beta(s_p)$ sufficiently small (using $\eta_2 \in Q_{s_p}$, which implies $|\eta_2| < \eta_3$). Therefore, solutions intersecting the D_{s_p} boundary of Q_{s_p} leave Q_{s_p} immediately.

The flow enters Q_{s_p} along the L_{s_p} boundary if

$$\dot{\eta}_2|_{\{\eta \in L_{s_p}\}} - \dot{\eta}_3|_{\{\eta \in L_{s_p}\}} < 0. \quad (\text{B27})$$

Since

$$\begin{aligned} \dot{\eta}_2|_{\{\eta \in L_{s_p}\}} &= \epsilon \eta_3^2 \{ \bar{S}_\perp[x(s_p), y(s_p)] + \eta_3 h_7 + \epsilon h_8 \}, \\ \dot{\eta}_3|_{\{\eta \in L_{s_p}\}} &= \epsilon \eta_3^2 \{ \bar{C}[x(s_p), y(s_p)] + \epsilon \eta_3 h_9 + \eta_3 h_{11} \} \end{aligned}$$

for Eq. (B27) to be true, we must have

$$\{ \bar{S}_\perp[x(s_p), y(s_p)] - \bar{C}[x(s_p), y(s_p)] \} + \eta_3 f_1 + \epsilon f_2 < 0, \quad (\text{B28})$$

where $f_i(\eta_3, \epsilon, t), i=1,2$ are smooth bounded functions. Since $\bar{S}_\perp[x(s_p), y(s_p)] - \bar{C}[x(s_p), y(s_p)] < 0$, the inequality (B28) can be satisfied by choosing ϵ and $\beta(s_p)$ sufficiently small as before. Since \mathcal{I} is compact, we can choose

$$\beta(s) \equiv \min_{s_p \in \mathcal{I}} \beta(s_p) = \beta,$$

so that inequalities (B26) and (B28) are satisfied for all $s_p \in \mathcal{I}$.

We define a cone bundle ψ along γ by letting

$$\psi = \bigcup_{s \in \mathcal{I}} Q_s.$$

The boundary of ψ is formed by the following sets (see Fig. 14):

$$D = \bigcup_{s \in \mathcal{I}} D_s, \quad L = \bigcup_{s \in \mathcal{I}} L_s, \quad (\text{B29})$$

$$S_+ = Q_{s_+}, \quad S_- = Q_{s_-}.$$

The flow exits ψ along, say, S_+ provided

$$\begin{aligned} \dot{\eta}_1|_{\eta \in S_+} &= \epsilon \eta_3 \{ \bar{\pi}[\gamma(s_+)] \} \\ &+ \eta_2 \bar{S}_\perp \{ [x(s_p), y(s_p)] \} + \eta_2^2 h_3 + \epsilon \eta_3 h_4 > 0. \end{aligned}$$

This last inequality can be satisfied by choosing β sufficiently small. Similar conclusion holds for S_- .

From the above analysis, we conclude that solutions intersecting the $L-\gamma$ boundary of ψ enter ψ immediately, and those that intersect D and the S_\pm boundary leave ψ immediately.

We now fix the origin of our coordinate system at \mathbf{p} , so that in $[x(s_p), y(s_p)] = \mathbf{p}$ in the equations of motion (B23)–(B25).

Solutions staying in ψ in backward time converge to γ . Consider an initial position $(\eta_{10}, \eta_{20}, \eta_{30}) \in \psi$ at t_0 and denote the trajectory emanating from this initial position by $[\eta_1(t), \eta_2(t), \eta_3(t)]$. Integration of

$$\dot{\eta}_3 = \epsilon \eta_3^2 [\bar{C}(\mathbf{p}) + \epsilon \eta_3 h_9 + \eta_1 h_{10} + \eta_2 h_{11}]$$

along the trajectory gives

$$\frac{\eta_{30}}{\eta_3(t)} = 1 + \epsilon \eta_{30} \int_t^{t_0} [\bar{C}(\mathbf{p}) + \epsilon \eta_3 h_9 + \eta_1 h_{10} + \eta_2 h_{11}] d\tau. \quad (\text{B30})$$

Since the trajectory stays in ψ for all backward times, Eq. (B30) holds for all $t \leq t_0$. By choosing s_- and s_+ sufficiently small, we can bound $\eta_1(t)$ and $\eta_2(t)$ to arbitrary small values leading to the estimate

$$\begin{aligned} 1 + \epsilon \eta_{30} \int_t^{t_0} [\bar{C}(\mathbf{p}) + \epsilon \eta_3 h_9 + \eta_1 h_{10} + \eta_2 h_{11}] d\tau \\ > 1 + \epsilon \eta_{30} \int_t^{t_0} \frac{\bar{C}(\mathbf{p})}{2} d\tau. \end{aligned} \quad (\text{B31})$$

Then Eqs. (B30) and (B31) imply

$$\eta_3(t) \leq \frac{\eta_{30}}{1 + \epsilon \eta_{30} \frac{\bar{C}(\mathbf{p})}{2} (t_0 - t)}.$$

This allows us to conclude that

$$\lim_{t \rightarrow -\infty} \eta_3(t) = 0.$$

In other words, trajectories that never leave ψ in backward time will necessarily converge to the $\eta_3=0$ boundary of the cone ψ .

There exists solutions that stay in ψ for all backward times. We now show that there are nonzero solutions that stay in ψ for all $t \leq t_0$. We first note that the set

$$\Psi = \{(\boldsymbol{\eta}, t) \mid \boldsymbol{\eta} \in \psi, t \in \mathbb{R}\} \quad (\text{B32})$$

has the following properties:

- (i) On the boundary component

$$\partial\Psi^1 = \{(\boldsymbol{\eta}, t) \in \Psi \mid \boldsymbol{\eta} \in D \cup S_+ \cup S_-\} \quad (\text{B33})$$

of Ψ , the vector field $(\dot{\boldsymbol{\eta}}, \dot{t})$ points strictly inward in backward time.

- (ii) On the boundary component

$$\partial\Psi^2 = \{(\boldsymbol{\eta}, t) \in \Psi \mid \boldsymbol{\eta} \in L - \gamma_v\} \quad (\text{B34})$$

of Ψ , the vector field $(\dot{\boldsymbol{\eta}}, \dot{t})$ points strictly outward in backward time.

- (iii) The remaining boundary component $\partial\Psi^3 = \Psi - \partial\Psi^1 - \partial\Psi^2$ of Ψ is just the invariant piece of the plane (γ_v, t) in the $(\boldsymbol{\eta}, t)$ space.
- (iv) As a consequence of (i)–(iii), the set of points immediately leaving Ψ in backward time is $W^{\text{im}} = \partial\Psi^2$.
- (v) Let W^{ev} denote the set of points eventually leaving Ψ in backward time. By definition, $W^{\text{im}} \subset W^{\text{ev}}$. Because $\partial\Psi^3$ is not in W^{ev} , we conclude that W^{im} is relatively closed in W^{ev} , i.e., any Cauchy sequence in W^{im} that does not have a limit in W^{im} will not have a limit in W^{ev} either.
- (vi) Ψ is a closed set in the $(\boldsymbol{\eta}, t)$ space.

The properties (iv)–(vi) of Ψ are the defining properties of a backward time Wasewsky set (see Appendix B 2 a). Recall that for any Wasewsky set, the Wasewsky map given by Eq. (B19) is continuous.

Suppose now that all nonzero solutions leave Ψ eventually in backward time. Then $W^{\text{ev}} = \Psi - \partial\Psi^3$, and hence $\Gamma(\Psi - \partial\Psi^3) = \partial\Psi^2$. But a continuous map Γ cannot map a connected set $\Psi - \partial\Psi^3$ into a disconnected set $\partial\Psi^2$, thus we obtain a contradiction. Therefore, there exist solutions that stay in ψ for all backward times, and these solutions converge to the $\xi=0$ as $t \rightarrow -\infty$. This proves the existence of the unstable manifold $W^u(t)$ for γ_v .

The unstable manifold $W^u(t)$ cannot be one dimensional because that would make W^{ev} a connected set, thereby violating the continuity of the Wasewsky map (B19). But $W^u(t)$ cannot be 3D either because that would violate the local volume-preserving property of the flow map [infinitesimal volumes tangent to $W^u(t)$ at the wall would shrink to zero in backward time, violating local incompressibility at the wall]. Thus, $W^u(t)$ must be a connected two-dimensional set depending smoothly on t .

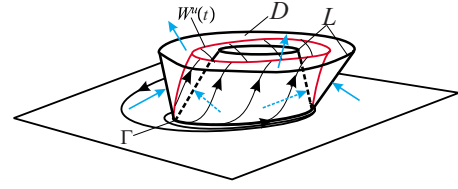


FIG. 15. (Color online) Wasewski set for a limit cycle.

d. Persistence of separation surfaces based at limit cycles

Let the trajectory $\mathbf{x}(s, \mathbf{x}_0)$ be contained in a limit cycle $\Gamma(s)$ of the averaged wall-shear field; assume that $\Gamma(s)$ has period T . Following the construction in Appendix B 2 c, we define a cone section along $\Gamma(s)$,

$$Q_{s_p} = \{(\eta_1, \eta_2, \eta_3) \mid \eta_1 = 0, |\eta_2| \leq \eta_3, 0 \leq \eta_3 \leq \beta(s_p)\},$$

where $\beta(s)$ is a positive continuous functions to be selected below (Fig. 15). The lateral side L_{s_p} of this cone is

$$L_{s_p} = \{(\eta_1, \eta_2, \eta_3) \in Q_{s_p} \mid |\eta_2| = \eta_3\},$$

and the top D_{s_p} is given by

$$D_{s_p} = \{(\eta_1, \eta_2, \eta_3) \in Q_{s_p} \mid \eta_3 = \beta(s_p)\}.$$

Based on an argument similar to the one given in Appendix B 2 c, we conclude that there exists $\beta(s_p) > 0$ and ϵ sufficiently small such that

$$\dot{\eta}_3|_{\{\boldsymbol{\eta} \in D_{s_p}\}} > 0$$

and

$$\dot{\eta}_2|_{\{\boldsymbol{\eta} \in L_{s_p}\}} - \dot{\eta}_3|_{\{\boldsymbol{\eta} \in L_{s_p}\}} < 0 \quad (\text{B35})$$

for all s_p . Choosing

$$\beta(s) \equiv \min_{s_p \in \mathcal{I}} \beta(s_p) = \beta,$$

we define a cone bundle ψ on $\Gamma(s)$,

$$\psi = \bigcup_{s \in \mathcal{I}} Q_s.$$

Again, the boundary of ψ is formed by the following sets:

$$D = \bigcup_{s \in \mathcal{I}} D_s, \quad L = \bigcup_{s \in \mathcal{I}} L_s. \quad (\text{B36})$$

With these ingredients, an estimate similar to the one used in Appendix B 2 c shows that solutions staying in ψ in backward time converge to Γ . We can then again invoke the Wasewsky principle to conclude that there exist solutions that stay in ψ forever in backward time. Then, following the arguments given in Appendix B 2 c, we again conclude the existence of a two-dimensional unstable manifold for Γ .

APPENDIX C: SEPARATION AT CORNERS

If the flow admits a corner at the intersection of the $z=0$ and $x=0$ planes, then by the no-slip condition along these two planes, the velocity field can be written as

$$\mathbf{v}(\mathbf{x}, z, t) = (xzA, xzB, xzC), \quad (\text{C1})$$

where

$$A(\mathbf{x}, z, t) = \int_0^1 \int_0^1 \partial_{xz}^2 u(rx, y, sz, t) dr ds,$$

$$B(\mathbf{x}, z, t) = \int_0^1 \int_0^1 \partial_{xz}^2 v(rx, y, sz, t) dr ds,$$

$$C(\mathbf{x}, z, t) = \int_0^1 \int_0^1 \partial_{xz}^2 w(rx, y, sz, t) dr ds.$$

After the change of coordinates

$$x = \bar{x}E_x(y, \bar{z}, t),$$

$$z = \bar{z}E_z(\bar{x}, y, t),$$

$$E_x(y, \bar{z}, t) = e^{\int_{t_0}^t \bar{z}E_z(\bar{x}, y, \tau)A(0, y, \bar{z}E_z(\bar{x}, y, \tau))d\tau},$$

$$E_z(\bar{x}, y, t) = e^{\int_{t_0}^t \bar{x}E_x(y, \bar{z}, \tau)C(\bar{x}E_x(y, \bar{z}, \tau), y, 0, \tau)d\tau},$$

the x -component of the equations of motion becomes

$$\begin{aligned} \dot{x} &= [\dot{\bar{x}} + \bar{x}\bar{z}E_zA(0, y, \bar{z}E_z)]E_x \\ &= \bar{x}\bar{z}E_xE_zA[\bar{x}E_x(y, \bar{z}, t), y, \bar{z}E_z(\bar{x}, y, t), t], \end{aligned}$$

or equivalently,

$$\begin{aligned} \dot{\bar{x}} &= \bar{x}\bar{z}E_z\{A[\bar{x}E_x(y, \bar{z}, t), y, \bar{z}E_z(\bar{x}, y, t), t] - A(0, y, \bar{z}E_z)\} \\ &= \bar{x}^2\bar{z}E_xE_z\{\partial_x A[0, y, \bar{z}E_z(\bar{x}, y, t), t] + \mathcal{O}(\bar{x})\}. \end{aligned}$$

The \bar{z} -component of the equations of motion is similar, with the role of \bar{x} and \bar{z} interchanged. The full set of transformed equations of motion is of the form

$$\dot{\bar{x}} = \bar{x}^2\bar{z}A_1(\bar{x}, y, \bar{z}, t),$$

$$\dot{y} = \bar{x}\bar{z}B_1(\bar{x}, y, \bar{z}, t),$$

$$\dot{\bar{z}} = \bar{x}\bar{z}^2C_1(\bar{x}, y, \bar{z}, t),$$

where

$$A_1(\bar{x}, y, \bar{z}, t) = E_xE_z[\partial_x A(0, y, \bar{z}E_z) + \mathcal{O}(\bar{x})],$$

$$B_1(\bar{x}, y, \bar{z}, t) = E_xE_zB(\bar{x}E_x, y, \bar{z}E_z, t),$$

$$C_1(\bar{x}, y, \bar{z}, t) = E_xE_z[\partial_z C(\bar{x}E_x, y, 0, t) + \mathcal{O}(\bar{z})].$$

Rescaling $\bar{z} \rightarrow \epsilon\bar{z}$ in order to focus on the dynamics near the $z=0$ boundary, we obtain

$$\dot{\boldsymbol{\eta}} = \boldsymbol{\epsilon}\mathbf{f}(\boldsymbol{\eta}, t) + \epsilon^2\mathbf{g}(\boldsymbol{\eta}, t; \epsilon), \quad (\text{C2})$$

where $\boldsymbol{\eta} = (\bar{x}, y, \bar{z})$ and

$$\mathbf{f} = \begin{pmatrix} \bar{x}^2\bar{z}A_1(\bar{x}, y, 0, t) \\ \bar{x}\bar{z}B_1(\bar{x}, y, 0, t) \\ \bar{x}\bar{z}^2C_1(\bar{x}, y, 0, t) \end{pmatrix},$$

$$\mathbf{g} = \begin{pmatrix} \bar{x}^2\bar{z}^2[\partial_z A_1(0, y, 0, t) + \mathcal{O}(\epsilon\bar{z}^2)] \\ \bar{x}\bar{z}^2[\partial_z B_1(\bar{x}, y, 0, t) + \mathcal{O}(\epsilon\bar{z}^2)] \\ \bar{x}\bar{z}^3[\partial_z C_1(\bar{x}, y, 0, t) + \mathcal{O}(\epsilon\bar{z}^2)] \end{pmatrix}.$$

We isolate the mean of \mathbf{f} via the averaging transformation,

$$\boldsymbol{\eta} = \boldsymbol{\zeta} + \epsilon\mathbf{w}(\boldsymbol{\zeta}, t),$$

$$\mathbf{w}(\boldsymbol{\zeta}, t) = \int_{t_0}^t [\mathbf{f}(\boldsymbol{\zeta}, \tau) - \bar{\mathbf{f}}(\boldsymbol{\zeta})]d\tau, \quad (\text{C3})$$

$$\bar{\mathbf{f}}(\boldsymbol{\zeta}) = \lim_{T \rightarrow \infty} \frac{1}{T} \int_{t_0-T}^{t_0} \mathbf{f}(\boldsymbol{\zeta}, \tau)d\tau,$$

which transform Eq. (C2) to the first-order averaged normal form,

$$\dot{\boldsymbol{\zeta}} = \boldsymbol{\epsilon}\bar{\mathbf{f}}(\boldsymbol{\zeta}) + \mathcal{O}(\epsilon^2), \quad (\text{C4})$$

which is analogous to Eq. (19). The steady limit of Eq. (C4) in component form is then given by Eq. (36).

APPENDIX D: REFINED SEPARATION SLOPE ESTIMATE

In order to obtain a refined estimate for the slope of separation curves and surfaces, we apply the slope formulas for steady separation derived by Surana *et al.*¹ to the steady limit,

$$\dot{\mathbf{r}} = \epsilon s[\bar{\boldsymbol{\tau}}(\mathbf{r}) + s\bar{\boldsymbol{\epsilon}}\bar{\mathbf{F}}(\mathbf{r})], \quad (\text{D1})$$

$$\dot{s} = \epsilon s^2[\bar{C}(\mathbf{r}) + s\bar{\epsilon}\bar{G}(\mathbf{r})],$$

of the second-order averaged system (A2). First note that at $t=t_0$, we have $z=\bar{z}$, therefore

$$(\mathbf{r}, s) = (\mathbf{q}, p) + \mathcal{O}(\epsilon^2) = (\mathbf{x}, z/\epsilon) + \mathcal{O}(\epsilon).$$

In the (\mathbf{x}, z) coordinates, therefore, the slope of a separation or attachment curve at the point $(\mathbf{p}, 0)$ is given by

$$\mathbf{g}_0 = -[\nabla_x \bar{\boldsymbol{\tau}}(\mathbf{p}) - \mathbf{I}\bar{C}(\mathbf{p})]^{-1}\bar{\mathbf{F}}(\mathbf{p}). \quad (\text{D2})$$

Note that

$$\begin{aligned} & \lim_{T \rightarrow \infty} \frac{1}{T} \int_{t_0-T}^{t_0} \mathbf{A}_1(\mathbf{q}, 0, \tau)\psi d\tau \\ &= \lim_{T \rightarrow \infty} \frac{1}{T} \left\{ [\phi\psi]_{t_0-T}^{t_0} - \int_{t_0-T}^{t_0} \phi[C_1(\mathbf{q}, 0, \tau) - \bar{C}]d\tau \right\} \\ &= - \lim_{T \rightarrow \infty} \frac{1}{T} \left\{ \int_{t_0-T}^{t_0} \phi[C_1(\mathbf{q}, 0, \tau) - \bar{C}]d\tau \right\}, \end{aligned}$$

where we have used $\bar{\boldsymbol{\tau}}(\mathbf{p})=0$ and the uniform boundedness of ϕ and ψ . We thus obtain the following simplified form of $\bar{\mathbf{F}}$ at the separation point:

$$\bar{\mathbf{F}}(\mathbf{p}) = \lim_{T \rightarrow \infty} \frac{1}{T} \int_{t_0-T}^{t_0} \left\{ \partial_z \mathbf{A}_1(\mathbf{q}, 0, t) + [\nabla_x \mathbf{A}_1(\mathbf{p}, 0, \tau) - C_1(\mathbf{p}, 0, \tau) \mathbf{I}] \int_{t_0}^{\tau} \mathbf{A}_1(\mathbf{p}, 0, s) ds \right\} d\tau.$$

Substituting this relation into Eq. (D2), we obtain the desired separation slope formula (41).

Applying the results of Surana *et al.*¹ to the steady flow (D1), we obtain that the slope of the separation surface at a point \mathbf{x}_0 of a separation line γ at time t_0 is given by

$$\tan[\theta(\mathbf{x}_0, t_0)] = - \lim_{s \rightarrow \infty} \int_0^s E(q) \frac{\bar{\mathbf{F}} \cdot \bar{\boldsymbol{\omega}}}{|\bar{\boldsymbol{\omega}}|} \Big|_{\mathbf{x}=\mathbf{x}(q, \mathbf{x}_0)} dq, \quad (\text{D3})$$

where the exponential $E(q)$ is defined by Eq. (44). Similarly, an attachment surface's slope satisfies

$$\tan[\theta(\mathbf{x}_0, t_0)] = - \lim_{s \rightarrow \infty} \int_0^s E(q) \frac{\bar{\mathbf{F}} \cdot \bar{\boldsymbol{\omega}}}{|\bar{\boldsymbol{\omega}}|} \Big|_{\mathbf{x}=\mathbf{x}(q, \mathbf{x}_0)} dq. \quad (\text{D4})$$

The quantity $\bar{\mathbf{F}} \cdot \bar{\boldsymbol{\omega}}$ appearing in the above slope formulas can be further simplified to

$$\begin{aligned} \bar{\mathbf{F}} \cdot \bar{\boldsymbol{\omega}} &= \lim_{T \rightarrow \infty} \frac{1}{T} \int_{t_0-T}^{t_0} \mathbf{F}(\mathbf{r}, \tau) \cdot \bar{\boldsymbol{\omega}} d\tau \\ &= \lim_{T \rightarrow \infty} \frac{1}{T} \int_{t_0-T}^{t_0} \{ \bar{\boldsymbol{\omega}} \cdot ([\nabla_x \mathbf{A}_1 - \bar{C} \mathbf{I}] \phi) + \psi \mathbf{A}_1 \cdot \bar{\boldsymbol{\omega}} \\ &\quad + \partial_z \mathbf{A}_1 \cdot \bar{\boldsymbol{\omega}} - \bar{\boldsymbol{\omega}} \cdot (\nabla_x \phi \bar{\boldsymbol{\tau}}) \} d\tau. \end{aligned}$$

Note that

$$\begin{aligned} &\lim_{T \rightarrow \infty} \frac{1}{T} \int_{t_0-T}^{t_0} \psi \mathbf{A}_1(\mathbf{q}, 0, \tau) \cdot \bar{\boldsymbol{\omega}} d\tau \\ &= \lim_{T \rightarrow \infty} \frac{1}{T} \left\{ [\psi \phi \cdot \bar{\boldsymbol{\omega}}]_{t_0-T}^{t_0} \right. \\ &\quad \left. - \int_{t_0-T}^{t_0} [C_1(\mathbf{q}, 0, \tau) - \bar{C}] \phi \cdot \bar{\boldsymbol{\omega}} d\tau \right\} \\ &= - \lim_{T \rightarrow \infty} \frac{1}{T} \left\{ \int_{t_0-T}^{t_0} [C_1(\mathbf{q}, 0, \tau) - \bar{C}] \phi \cdot \bar{\boldsymbol{\omega}} d\tau \right\}, \quad (\text{D5}) \end{aligned}$$

where we have used the identity $\bar{\boldsymbol{\tau}} \cdot \bar{\boldsymbol{\omega}} = 0$; we have also used the uniform boundedness of ϕ and ψ . As a consequence, we obtain

$$\begin{aligned} \bar{\mathbf{F}} \cdot \bar{\boldsymbol{\omega}} &= \lim_{T \rightarrow \infty} \frac{1}{T} \int_{t_0-T}^{t_0} \mathbf{F}(\mathbf{r}, \tau) \cdot \bar{\boldsymbol{\omega}} d\tau \\ &= \lim_{T \rightarrow \infty} \frac{1}{T} \int_{t_0-T}^{t_0} \left\{ \partial_z \mathbf{A}_1 \cdot \bar{\boldsymbol{\omega}} + \bar{\boldsymbol{\omega}} \cdot \left([\nabla_x \mathbf{A}_1 - C_1 \mathbf{I}] \right. \right. \\ &\quad \left. \left. \times \int_{t_0}^{\tau} [\mathbf{A}_1 - \bar{\boldsymbol{\tau}}] dp \right) - \bar{\boldsymbol{\omega}} \cdot \left(\int_{t_0}^{\tau} [\nabla_x \mathbf{A}_1 - \nabla_x \bar{\boldsymbol{\tau}}] dp \bar{\boldsymbol{\tau}} \right) \right\} d\tau, \quad (\text{D6}) \end{aligned}$$

which makes Eqs. (D3) and (D4) equivalent to the slope formulas given in Eqs. (43) and (45).

¹A. Surana, O. Grunberg, and G. Haller, "Exact theory of three-dimensional separation. Part I: Steady separation," *J. Fluid Mech.* **564**, 57 (2006).

²M. Tobak and D. J. Peake, "Topology of three-dimensional separated flows," *Annu. Rev. Fluid Mech.* **14**, 61 (1982).

³G. T. Chapman, "Topological classification of flow separation on three-dimensional bodies," AIAA Paper No. 86-0485, 1986.

⁴R. L. Simpson, "Aspects of turbulent boundary layer separation," *Prog. Aerosp. Sci.* **32**, 457 (1996).

⁵J. M. Déclery, "Robert Legendre and Henri Werlé: Toward the elucidation of three-dimensional separation," *Annu. Rev. Fluid Mech.* **33**, 129 (2001).

⁶G. Haller and A. Poje, "Finite-time transport in aperiodic flows," *Physica D* **119**, 352 (1998).

⁷G. Haller, "Finding finite-time invariant manifolds in two-dimensional velocity fields," *Chaos* **10**, 99 (2000).

⁸G. Haller, "Exact theory of unsteady separation for two-dimensional flows," *J. Fluid Mech.* **512**, 257 (2004).

⁹S. F. Shen, "Unsteady separation according to the boundary layer equations," *Adv. Appl. Mech.* **13**, 177 (1978).

¹⁰L. L. Van Dommelen and S. F. Shen, "The genesis of separation," in *Proceedings: Symposium on Numerical and Physical Aspects of Aerodynamic Flows*, Long Beach, CA, 19–21 January 1981, edited by T. Cebici (Springer, New York, 1982), pp. 293–311.

¹¹L. L. Van Dommelen and S. J. Cowley, "On the Lagrangian description of unsteady boundary layer separation, Part 1. General theory," *J. Fluid Mech.* **210**, 593 (1990).

¹²C. S. Liu and Y. H. Wan, "A simple exact solution of the Prandtl boundary layer equations containing a point of separation," *Arch. Ration. Mech. Anal.* **89**, 177 (1985).

¹³W. E. and B. Engquist, "Blowup of solutions of unsteady Prandtl's equation," *Commun. Pure Appl. Math.* **50**, 1287 (1997).

¹⁴J. Z. Wu, R. W. Tramel, F. L. Zhu, and X. Y. Yin, "A vorticity dynamics theory of three-dimensional flow separation," *Phys. Fluids* **12**, 1932 (2000).

¹⁵J. Z. Wu, H. Y. Ma, and M. D. Zhou, *Vorticity and Vortex Dynamics* (Springer, New York, 2006).

¹⁶M. S. Kilic, G. Haller, and A. Neishtadt, "Unsteady flow separation by the method of averaging," *Phys. Fluids* **17**, 067104 (2005).

¹⁷J. A. Sanders and F. Verhulst, *Averaging Methods for Nonlinear Dynamical Systems* (Springer, New York, 1985).

¹⁸A. Surana, "Nonlinear dynamics of three dimensional fluid flow separation," Ph.D. thesis, Massachusetts Institute of Technology, 2007.

¹⁹D. J. Peake and M. Tobak, "Topological structure of three-dimensional separated flows," AIAA Paper No. 81-1260, 1981.

²⁰W. R. Sears and D. P. Tellionis, "Boundary-layer separation in unsteady flow," *SIAM J. Appl. Math.* **28**, 215 (1975).

²¹J. W. Elliott, F. T. Smith, and S. J. Cowley, "Breakdown of boundary layers: (i) on moving surfaces; (ii) in semi-similar unsteady flow; (iii) in fully unsteady flow," *Geophys. Astrophys. Fluid Dyn.* **25**, 77 (1983).

²²A. Surana and G. Haller, "Ghost manifolds in slow-fast systems, with applications to unsteady fluid flow separation," *Physica D* **237**, 1507 (2008).

²³A. Surana, G. Jacobs, and G. Haller, "Extraction of separation and attachment surfaces from 3D steady shear flows," *AIAA J.* **45**, 1290 (2007).

²⁴A. E. Perry and M. S. Chong, "A series expansion study of the Navier-Stokes equations with applications to three-dimensional separation patterns," *J. Fluid Mech.* **173**, 207 (1986).

²⁵A. Spohn and P. Gillieron, "Flow separations generated by a simplified geometry of an automotive vehicle," in *Proceedings of the IUTAM Symposium on Unsteady Separated Flows*, Toulouse, France, 8–12 April 2002, edited by M. Braza, C. Hirsch, and F. Hussain.

²⁶P. N. Shankar and M. D. Deshpande, "Fluid mechanics in the driven cavity," *Annu. Rev. Fluid Mech.* **32**, 93 (2000).

²⁷G. Haller, "An objective definition of a vortex," *J. Fluid Mech.* **525**, 1 (2005).

²⁸C. Conley, *Isolated Invariant Set and Morse Index* (American Mathematical Society, Providence, 1970).